

DESCRIPTION OF THE DIGIT-FOOSH-COPS SPECTROSCOPIC DATA PIPELINE AND PRODUCTS

JOEL D. GREEN, YAO-LUN YANG, NEAL J. EVANS, II, AGATA KARSKA, GREGORY
HERCZEG, EWINE F. VAN DISHOECK, JEONG-EUN LEE, & JEROEN BOUWMAN

1 Abstract

This report documents the DIGIT-FOOSH-COPS *Herschel* spectroscopy data products. The products include datacubes, contour maps, automated line fitting results, and best 1-D spectra products for all protostellar and disk sources observed with PACS in RangeScan mode for two observing programs: the DIGIT Open Time Key Program (30 sources; KPOT_nevans_1 and SDP_nevans.1; PI: N. Evans), and the FOOSH Open Time Program (6 sources; OT1_jgreen02.2; PI: J. Green). In addition, we provide our best SPIRE-FTS spectroscopic products for the COPS Open Time Program (OT2_jgreen02.6; PI: J. Green) and FOOSH sources. We include details of data processing, descriptions of output products, and tests of their reliability for user applications. We describe additional by-hand corrections performed post-processing, and identify the parts of the dataset to be used with caution. We include our full source list in a table. For the first time, this uniformly reduced dataset will allow us to categorize securely the far-infrared to sub-millimeter wavelength spectral properties of young stars in nearby star-forming regions.

2 Introduction

This document describes the delivery of *Herschel*-PACS and SPIRE spectroscopic observations of 70 objects (protostars, young stellar objects, and FU Orionis objects) from the “Dust, Ice, and Gas in Time” (DIGIT Key Project), “FU Orionis Objects Surveyed with *Herschel*” (FOOSH OT1), and “CO in Protostars” (COPS OT2) *Herschel* programs. We use data products from the HIPE 13 / CalTree 65 pipeline, provided by the *Herschel* Science Center, the most current version at the time of reprocessing during summer 2014. The main new feature of the PACS spectroscopy is a correction for pointing and jitter offsets during observations. The SPIRE spectra include the correction for extended sources. In addition to this document, information on this archive will be found in forthcoming papers on the full dataset (Green et al., in prep.) and on 3-D radiative transfer modeling of a single source (the protostar BHR71; Yang et al., in prep.). The corresponding *Spitzer* data can mostly be found in IRS_Disks and c2d programs.

3 Observations

3.1 Dust, Ice, and Gas In Time (DIGIT)

The full DIGIT spectroscopic sample consists of 63 sources: 24 Herbig Ae/Be stars (intermediate mass sources with circumstellar disks), 9 T Tauri stars (low mass young stars

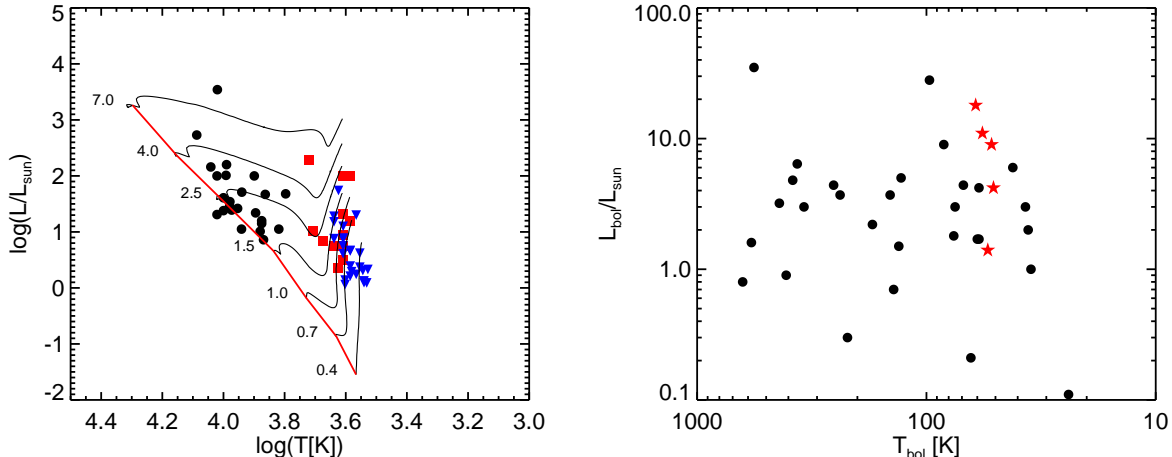


FIGURE 1: **Left:** Range of stellar temperature and L_{bol} for the disk sample, superimposed on the HR diagram with evolutionary tracks by Palla & Stahler (1993). The filled black circles indicate our Herbig Ae sample, the red squares indicate the HR diagram positions of our CTTS sample, and the blue triangles denote the positions of our WTTS sample. **Right:** Range of T_{bol} and L_{bol} for the embedded sample. Red stars indicate sources observed by WISH with PACS full spectral scans.

with circumstellar disks), and 30 protostars (young stars with significant envelope emission) observed with PACS spectroscopy. The distribution in luminosity and characteristic temperature are shown in Figure 1. The WTTS sample was observed photometrically and delivered separately. It is fully described by Cieza et al. (2013).

An earlier data reduction procedure was used in a summary of the embedded protostar sample in Green et al. (2013b). The 30 object protostar sample was drawn from previous studies (summarized by Lahuis et al. 2006), focusing on protostars with high-quality *Spitzer*-IRS 5-40 μm and UV, optical, infrared, and submillimeter complementary data. The protostars were selected to span two orders of magnitude in bolometric luminosity and bolometric temperature, while the disk sources were selected as bright targets for PACS spectral scans.

The full DIGIT embedded protostellar sample consisted of 30 Class 0/I targets. Two sources (IRS44 and IRS46) were observed in a single pointing centered on IRS46. These objects are selected from some of the nearest and best-studied molecular clouds: Taurus (140 pc; 6 targets), Ophiuchus (125 pc; 7 targets), Perseus (230-250 pc; 7 targets), R Corona Australis (130 pc; 3 targets), Serpens (429 pc; 2 targets), Chamaeleon (178 pc, 1 target), and 4 additional isolated cores. The sources span two orders of magnitude in luminosity, from 0.11 to 27.8 L_{\odot} , with bolometric temperatures spanning the Class 0/I divide from 27 to 592 K. Their photometry fluxes at 100 μm span two orders of magnitude as well, from 1.0 to 240.1 Jy. Their $L_{\text{bol}}/L_{\text{smm}}$ ranges from 5 to > 10000 , with most (18/22 with well-constrained submm data) falling between 10 and 1000.

PACS is a 5×5 array of $9.4'' \times 9.4''$ spatial pixels (hereinafter referred to as “spaxels”) covering the spectral range from 50-210 μm with $\lambda/\Delta\lambda \sim 1000$ -3000, divided into four

segments, covering $\lambda \sim 50\text{-}75, 70\text{-}105, 100\text{-}145, \text{ and } 140\text{-}210 \mu\text{m}$. The PACS spatial resolution ranges from $\sim 9''$ at the shortest wavelengths ($50 \mu\text{m}$) to $\sim 18''$ at the longest ($210 \mu\text{m}$). The nominal pointing RMS of the telescope is $2''$. However, targets observed during certain periods show consistently greater offsets (see below).

For the DIGIT embedded protostars sample we utilized the full range of PACS ($50\text{-}210 \mu\text{m}$) in two linked pointed chop/nod rangescans: a blue scan covering $50\text{-}75$ and $100\text{-}150 \mu\text{m}$ (SED B2A + short R1); and a red scan covering $70\text{-}105$ and $140\text{-}210 \mu\text{m}$ (SED B2B + long R1). We used 6 and 4 range repetitions respectively, for integration times of 6853 and 9088 seconds (a total of ~ 16000 seconds per target for the entire $50\text{-}210 \mu\text{m}$ scan). Excluding overhead, 50% of the integration time is spent on source and 50% on sky. Thus the effective on-source integration times are 3088 and 4180 seconds, for the blue and red scans, respectively. The total on-source integration time to achieve the entire $50\text{-}210 \mu\text{m}$ scan is then 7268 seconds.

The telescope and sky background emission was subtracted using two nod positions $6'$ from the source in opposite directions. The telescope chopped between the source and nod positions, cycling every $1/8$ of a second in a pre-determined pattern of on and off positions (Poglitsch et al., 2010) during the integration.

21 of the 33 disk sources were observed with the same procedure as the embedded objects. The other 12 sources were only partially covered: 8 Herbig Ae/Be sources (HD 35187, HD 203024, HD 245906, HD 142666, HD 144432, HD 141569, HD98922, and HD 150193) and 4 T Tauri sources (HT Lup, RU Lup, RY Lup, and RNO90) were observed using *only* the blue scans (i.e. achieving a wavelength coverage only from SED B2 + short R1). 9 of these 12 sources (all except HD 35187, HD 203024, and HD 245906) were observed in a further limited wavelength range ($60\text{-}72 + 120 - 134 \mu\text{m}$; referred to as “forsterite only” scans for their focus on the $69 \mu\text{m}$ forsterite dust feature). This procedure allowed shorter integration times to achieve the same SNR in the covered regions.

3.2 FU Orionis Objects Surveyed with Herschel (FOOSH)

FU Orionis-type objects (hereafter, FUors) are a class of low-mass pre-main sequence objects named after the archetype FU Orionis (hereafter, FU Ori), which produced a 6 magnitude outburst at B -band in 1936 and has remained close to peak brightness ever since. The FOOSH program consisted of 21 hrs of Herschel observing time: V1057 Cyg, V1331 Cyg, V1515 Cyg, V1735 Cyg, and FU Ori were observed as part of FOOSH and analyzed from preliminary data reduction (Green et al., 2013a).

For the FOOSH sample we again utilized the full range of PACS ($50\text{-}210 \mu\text{m}$) in two linked pointed chop/nod rangescans: a blue scan covering $50\text{-}75$ and $100\text{-}150 \mu\text{m}$ (SED B2A + short R1); and a red scan covering $70\text{-}105$ and $140\text{-}210 \mu\text{m}$ (SED B2B + long R1). We used 6 and 4 range repetitions respectively, for integration times of 3530 and 4620 seconds (a total of ~ 8000 seconds per target and off-positions combined, for the entire $50\text{-}210 \mu\text{m}$ scan; the on-source integration time is ~ 3000 seconds). The telescope sky background was subtracted using two nod positions $6'$ from the source.

The SPIRE-FTS data were taken in a single pointing with sparse image sampling, high

spectral resolution, in 1 hr of integration time. The spectrum is divided into two orders covering the spectral ranges $194 - 325 \mu\text{m}$ (“SSW”; Spectrograph Short Wavelengths) and $320 - 690 \mu\text{m}$ (“SLW”; Spectrograph Long Wavelengths), with a resolution, $\Delta\nu$ of 1.44 GHz and resolving power, $\lambda/\Delta\lambda \sim 300\text{--}800$, increasing at shorter wavelengths (Griffin et al., 2010).

3.3 CO in ProtoStars (COPS)

The sample of 31 “COPS” protostars observed with SPIRE-FTS includes 25 sources from the DIGIT and 6 from the WISH (Water in Star-forming regions with *Herschel*, PI: E. van Dishoeck; van Dishoeck et al. 2011; see also Nisini et al. 2010; Kristensen et al. 2012; Karska et al. 2013; Wampfler et al. 2013) key programs. A nearly identical sample was observed in CO $J = 16 \rightarrow 15$ with HIFI (PI: L. Kristensen) and is presented in Kristensen et al. (in prep.). This dataset (COPS: SPIRE-FTS) is analyzed in a forthcoming paper (Green et al., in prep.). The SPIRE beamsizes range from $17\text{--}40''$, equivalent to physical sizes of $\sim 2000\text{--}10000$ AU at the distances of the COPS sources, comparable to the size of a typical core (Ward-Thompson et al., 2007) but smaller than many collimated outflows.

The COPS SPIRE-FTS data were observed identically to the FOOSH SPIRE data, in a single pointing with sparse image sampling, high spectral resolution, in 1 hr of integration time per source.

3.4 Overview of the Products

The basic data products we produce for each source observed with PACS and SPIRE spectroscopy are the following:

- Extractions of the datacubes (wavelength vs. flux density vs. spatial position), with advanced corrections from HIPE 13.
- Best-calibration 1-D spectra for point sources and marginally extended sources within the data cube, including flat spectra (continuum-subtracted) and rebinned continuum (line subtracted) products.
- Line identification and fit parameters obtained with an automated fitting routine, organized by spatial position for each source, including a complete sortable linelist.
- Contour plots for extended line and continuum emission.
- EPS files for all above products, for users to track and verify all automated fits.

In this document, we review the archive data processing and products in detail. First we describe the custom data reduction pipeline we used. Second, we describe the data products and output file format, including post-processing data products. Third, we summarize the reliability of our products, and lastly we include our line source libraries and a full inventory of sources included in this archive.

4 Pipeline settings

4.1 PACS Pipeline for Pointlike and Small Sources

We begin with the `hipe13.0.1006.ChopNodPointingCorrection.py` pipeline script (the “Point Source Background Normalization” script. This was made available in HIPE 13; any version of HIPE 13 should work for this purpose. We then made the following modifications:

- The script is run as a loop over numerous OBSIDs for blue and red cameras.
- We make an adjustment in the pipeline to account for the effects of pointing jitter (changes in pointing offset during the course of the observation). The chi-squared difference between the flux of the “point” source and the flux of the centered beam, via a map/grid, is determined using the beams of calibration products. We define the “oversample” (the samples per spatial element in each dimension, improving precision of positional determination) and the “smoothFactor” (smoothing in the spectral domain, in terms of grating positions rather than wavelength). For the pipeline, we set these to `oversample = 8` and `smoothFactor = 7`; using larger values yielded no apparent benefit.
- In the `specFlatFieldRange` command, we decrease “polyOrder” to 4 (from the default of 5). This slightly improves memory usage, although the effect is minor.
- We select `excludeLeaks=True` so that we do not use the light-leakage affected regions for flatfielding. These regions are then not reported in the final spectrum at all, which removes the 95-105 μm range (and a few spectral lines in that region). The advantage to removing this data are that we avoid this typically erratic continuum region in the determination of the flatfielding correction. Any line fluxes determined from the 95-105 μm region should be used with caution, and the continuum level will be inaccurate.
- We change the “gaussianFilterWidth” to 35 (instead of 50). This parameter is the number of wavelength points over which we assess the scaling of the central spaxel to the level of the 3x3 spaxel set, which is used in the production of the “3x3YES” product, below; it is an attempt to correct for the shape of the continuum, picking a width large enough to account for pointing jitter but not so wide as to smooth out the actual continuum shape. By using the flux of the “3x3” central 9 spaxels, and comparing to a true point source distribution, we correct for the movement of the flux centroid throughout the observation, referred to as pointing jitter. The number is essentially based on the sampling and the significance of pointing jitter, for a particular observation; we settled on a value of 35 through trial-and-error testing, while slightly reducing the computational load on our processors.
- We add a “garbage collection” line at the end of the loop. This has allowed us to run at least 200 OBSIDs within the same command, given sufficient disk space. It takes about 1 hour/OBSID to run at these settings on a (early 2014) 12-core processor with 96 GB of RAM dedicated to the process, excluding data download time; for a total of

200 OBSIDs, we required 200 CPU hours (e.g., 2 weeks) to reduce ALL targets in our sample.

Earlier versions of the pipeline showed significant mismatches between red and blue modules, and frequently did not align with photometry or with SPIRE observations of the same position. The early pipelines did not fully account for source spatial extent or pointing jitter, and the relative spectral response function did not work well at the edges of each order. All of these effects are accounted for and the results have dramatically improved the continuum calibration for PACS in particular.

For example, consider the improvement to the continuum shape and absolute flux calibration shown for the protostar BHR71. Our new pipeline includes updated calibration data, improved flatfielding, and jitter correction, and other small improvements noted earlier. Table 1 and Figure 2 show the improvement numerically and graphically, respectively. Our best products from the new pipeline results match very closely with photometry on select sources. The photometry data are extracted from archival *Herschel* observations with the same source size indicated by the HIPE pipeline.

The improvement from the jitter correction is shown (for TMR1) in Figure 3. The jitter correction (red) has removed several spurious broad features and improved overall flux calibration when compared with the non-corrected spectrum (black). The overall flux level of the new spectrum is closer to photometric values obtained in separate observations.

TABLE 1: Percent Difference Between Photometry and Spectrometry for BHR71

Wavelength	< 2014 Reduction	2014 Reduction
μm	%	%
70	8.3	4.2
100	27.0	8.3
160	24.4	11.9

Note. —The disparity of PACS spectroscopy, relative to photometry measured in a single aperture size (24.5"), for case study BHR71. The < 2014 Reduction column compares the absolute flux density measured from the previous (Green et al., 2013b) reduction techniques to PACS photometry at the same wavelength; the 2014 Reduction column compares our most recent updated methods described herein to the same photometry. The new reduction techniques are a much closer match to the photometry. This is shown graphically in Figure 2.

Among the embedded sources in our sample, we got very poor results from the jitter correction on 14 sources: IRAM 04191, L1014, L1455-IRS3, RCrA-IRS5A, RCrA-IRS7C, IRS 46, Serpens-SMM4, EC 82, HD 98922, HD 245906, HD 203024, HT Lup, HD 142666, and HD 35187. These sources all have complicated PACS fields in which the central source is

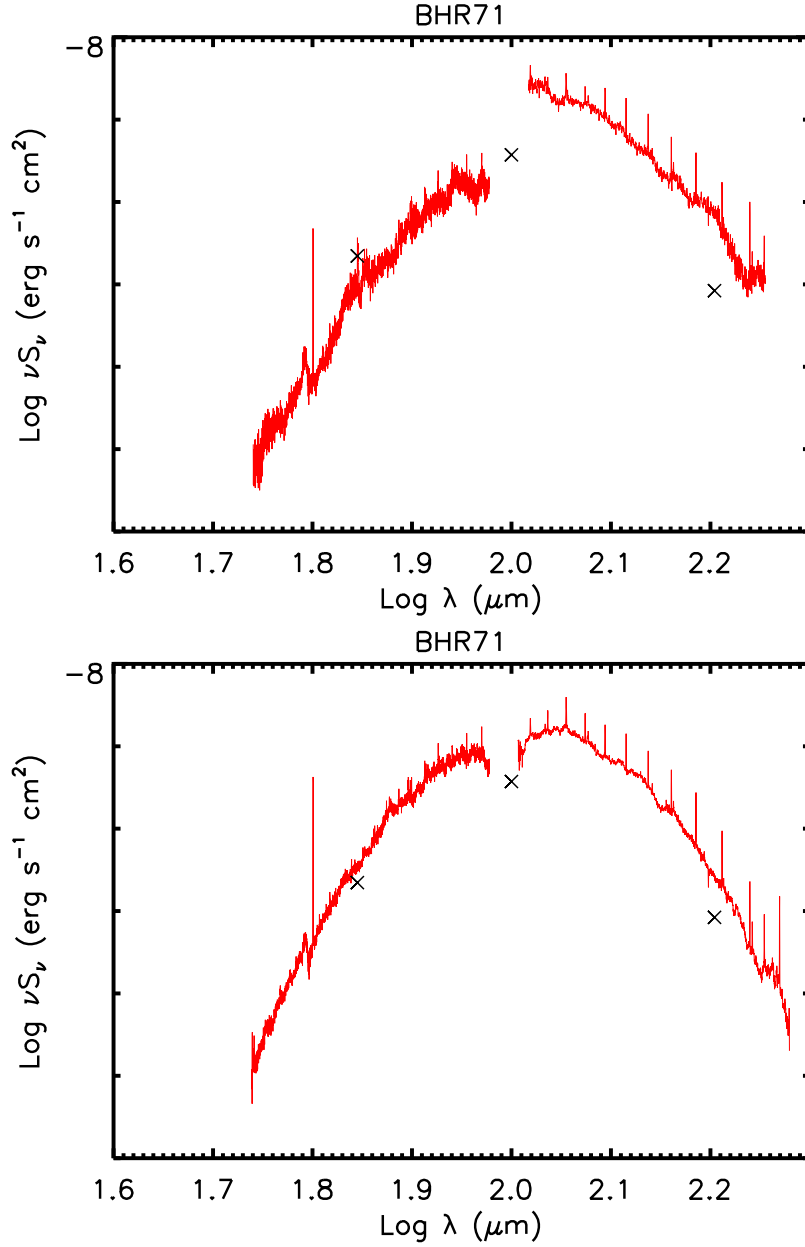


FIGURE 2: Before and after new techniques. The plot on the top shows the old reduction without scaling. Photometric data (labeled by \times symbols) obtained later shows a substantial discrepancy. The plot of the bottom shows the results of the new reduction which produces smoother spectra and better agreement with photometry. The flatfield corrections have removed most of the false “solid-state features.”

not the brightest object, or have weak continuum (< 3 Jy at $60 \mu\text{m}$); for these seven objects, we include only the “non-jitter corrected” versions in our archive. In two embedded sources, we found significant (10%) flux mismatches between the two OBSIDs merged to form the

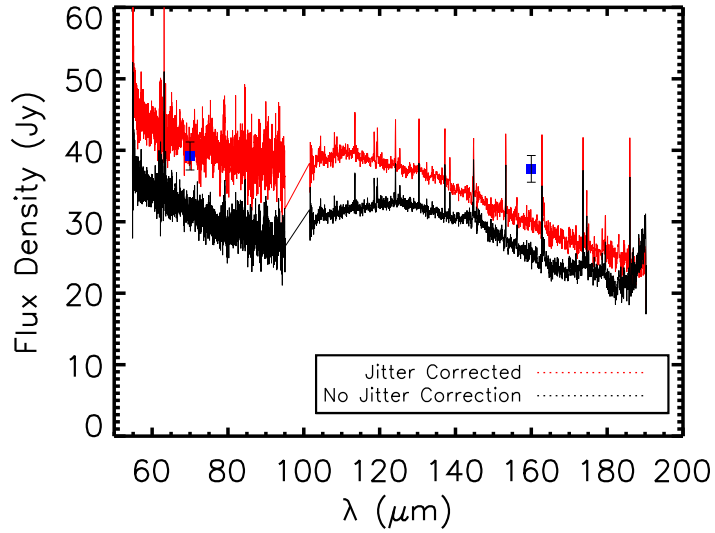


FIGURE 3: Application of the “jitter correction” in the PACS pipeline for TMR1, showing the improvement in spectral shape and continuum flux density calibration. The effect of the jitter correction (red) is shown in comparison to the uncorrected spectrum (black); the corrected spectrum is more consistent with PACS photometry (blue) extracted from a $34.5''$ radius aperture, with formal 5% errors; in addition, several spurious wide features are removed and the reliable long-wavelength continuum increases from $180 \mu\text{m}$ to $190 \mu\text{m}$. While an improvement, the correction still does not match the long wavelength photometry perfectly in this source.

spectrum of L1551-IRS5 (in which the observations were separated by 1.5 yr) and GSS30-IRS1 (which shows complicated behavior at long wavelengths; [Je et al. \(2015\)](#)). In addition, slight mismatches are noted in L1448-MM (a partially blended chain of sources; [Lee et al. 2013](#)). We find excellent flux matches between modules in all other sources, including all disk/point sources, even in cases with up to 0.5 spaxel mispointings (e.g. TMC1A, IRAS 12496, TMR1, and L1527). Note that there is no manual scaling applied after the pipeline reduction. The advanced pipeline with jitter correction matches the fluxes by matching the minor mispointings at different wavelengths.

4.2 SPIRE Pipeline for Pointlike and Semi-Extended Sources

Each order was reduced separately within HIPE version 13.0 using the standard pipeline for extended sources, including apodization. The apodization process corrects the sinc function line profiles to Gaussian line profiles and smooths the spectrum. Originally, SPIRE has a spectral resolution of 1.2 GHz. Because the signal are recorded in Fourier domain, the line would appear as a sinc function. With the apodization, the spectra become smooth but the line widths become 50% wider than the width of the sinc function. SPIRE used an onboard calibration source for flux calibration.

The SPIRE data were extracted using the “extended source” calibration pipeline, as this produced a smoother continuum between modules, better signal-to-noise ratio (SNR), and fewer spectral artifacts than the “point source” pipeline. We performed post-processing within HIPE version 13.0.1006, using SPIRE calibration dataset 12. Starting from the baseline data products, we used the “SemiExtendedSourceCorrector” script, which uses the mismatch between SLW and SSW to determine an observed source size. This routine compares the SLW and SSW flux density pixel-by-pixel, and fits a single “aperture size” that produces the best match between modules, using a top-hat circular aperture overlaid on the SPIRE field-of-view. The routine then extracts the spectrum from SSW and SLW using this designated aperture and produces a single 1-D spectrum. No background subtraction was performed, and thus the spectrum should be considered an upper limit to the true flux density in one pixel. The routine then extracts a spectrum from the SPIRE-FTS datacube using an annulus of the derived size. An example product (TMR1) is shown in [Figure 4](#). Note that the “extended source” calibration of few sources (HH100, IRS46, and V1735 Cyg) are not provided due to their poor spectra qualities.

Thus unlike the PACS pipeline, no significant modifications were made to the basic pipeline script, except for allowing it to run in a loop and for the separate post-processing step using the extended source calibration script.

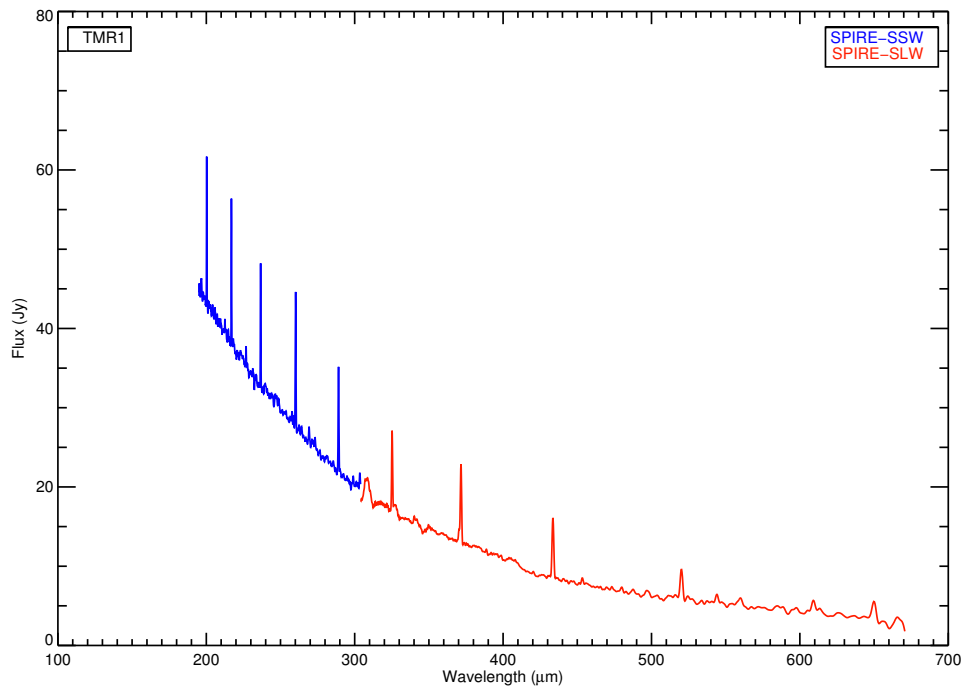


FIGURE 4: TMR1 SPIRE spectrum, with the SSW module (blue) and SLW module (red) corrected with the semi-extended source corrector. The SLW continuum shows a spurious feature at $300 \mu\text{m}$ which is trimmed during reduction.

5 Automated Line-Fitting

We use an automated emission line fitting process that tries to fit lines from a pre-existing database of laboratory wavelengths, identifies the threshold for detection, then generates tables of line flux, width, centroid, and uncertainties for every detected line, along with an upper limit to the flux for every undetected line for all PACS and SPIRE spectra in the sample. This information is then combined with spatial information for each pixel to produce contour maps including all spatial positions where significant detections are found. The line-fitting algorithm uses `mpfit`, a Levenberg-Marquardt non-linear least squares minimization (Markwardt, 2009), to determine emission line properties. After producing a line detection database, we test the integrity of the line fits to better characterize the SNR, decouple any blended lines, and produce easily searchable products for further science applications. The automated results have been spot checked by eye but should be used with caution. The detailed procedures are described in the following sections.

5.1 Line List

A comprehensive and pre-selected line list is used to supply initial fit parameters line-by-line for the automated routine. We require an expected line list to restrict our line fitting to specific regions of the spectrum, pre-select line-free continuum regions, and identify the lines after fitting. For this dataset, we verified that there were no significant unidentified lines. If the input spectrum contains a line that is not included in our list, one can easily check whether every significant feature has been extracted from the spectrum: any line not included in the linelist will then appear in the continuum-subtracted “flat” spectrum (see §5.2). The line list includes lines of ^{12}CO , ^{13}CO , H_2O , OH , HCO^+ , CH^+ , and atomic fine-structure transitions in the wavelength range of 55-670 μm (Tables 4, 5, 6, 7, and 8). There are two CH^+ lines, $\text{CH}^+ J = 4 - 3$ and $\text{CH}^+ J = 2 - 1$ that are excluded because they are heavily blended with nearby potentially strong lines (water lines). The laboratory data for each line was collected from the Leiden Atomic and Molecular Database (LAMDA; Schöier et al. 2005) and the Cologne Database for Molecular Spectroscopy (CDMS; Müller et al. 2005). However, the $^{12}\text{CO} J = 48 - 47$ to $^{12}\text{CO} J = 41 - 40$ lines were not included in LAMDA until recently; thus we calculated the frequency and Einstein-A coefficient using a method from Authier et al. (1993) and the model of the dipole matrix element in Goorvitch (1994). An updated CO extrapolation added to LAMDA (Neufeld, in prep.) agrees with our calculations. We use slightly different line centroids of OH lines adopting from Wampfler et al. (2013). The only difference is the line centroid of OH $^2\Pi_{1/2, 3/2}^+ - ^2\Pi_{1/2, 1/2}^-$. We use 163.12 μm instead of 163.019 μm from LAMDA. We used only subsets of the line list within the wavelength range of the observations for each specific source.

5.2 Baseline Selection and Fitting

Before fitting each line, a region of line-free spectrum from wavelengths near the theoretical line centroid (hereafter line-region) was determined and used for baseline fitting. The baseline fitting region is, by default, 20 times the spectral resolution at the wavelength of the

line centroid. However, some of these wavelengths may include other emission lines. Thus we used only line-free wavelengths (determined from our previously identified line list) until we had accumulated 10 times the spectral resolution, both blue-ward and red-ward of the line centroid. Then, we fitted the selected baseline region using a second order polynomial. Once we obtained a well-constrained baseline, we subtracted the baseline from the identified wavelength region. This continuum-subtracted spectrum was then used for line-fitting.

5.3 Line Selection and Fitting

We began with the baseline-subtracted spectrum. The next step was to extract the line profile, using a Gaussian model. Several constraints were applied to the fitting process of PACS and SPIRE spectra. When fitting PACS spectra, we initially allowed the line centroid to vary within ± 2 times the spectral resolution at the theoretical line centroid. However, the spectral resolution of PACS was insufficient to velocity-resolve most of the lines except for the [O I] line at $63.18 \mu\text{m}$. After comparing the fitting results with and without the line width fixed at PACS instrumental resolution, we found that both strong lines and weak lines can be found in fixed width setting with moderate SNR, while the flexible width setting produces better SNR on strong lines but might fit with a narrower feature than it should at some wavelengths. Therefore, for all lines other than [O I], we fixed the FWHM of the line to the PACS spectral resolution. Users might be able to achieve a higher SNR, but we adopted the fixed width setting to avoid fake lines of this archive. For SPIRE, similar problems are not found due to the higher oversampling rate; thus we kept all line widths flexible within $\pm 30\%$ of the SPIRE instrumental resolution. The instrumental resolution of PACS is obtained from personal communication with Helmut Feuchtgruber from MPE/Garching, and the instrumental resolution of SPIRE is obtained from SPIRE data reduction guide released by *Herschel*.

5.4 Blended Lines Fitting: Double Gaussian Fitting

Some emission lines are sufficiently blended that our default single Gaussian profile does not characterize the line shape. For known blended lines (Table 9), we used a double Gaussian function to fit the combined profile. The component blended line widths were fixed to the apodized spectral resolution. For blended lines, we require that both lines are in emission; if an absorption line is blended with an emission line, it cannot be fitted. When the fitting routine hit the boundary and tried to iterate toward negative height, the height of line would be set to zero resulting in a zero in the line strength on the report. In a few cases, a detected single line can feasibly be identified with either of two lines, depending on the physical properties or chemical composition of the source. For these cases, we used a simple criterion to identify the possible blended regions as well as the likely dominant line. For any pair of lines with centroids within one resolution element of each other, we classify the fit as a possible blended line, label the two options with Red and Blue indicating whether we attribute the blended line to the longer or shorter wavelength candidate. If a given line is not blended, we label it as x; if a line is blended with two other possible lines, the line is flagged

with Red/Blue. Our recommended line identification is simply the line with the highest Einstein-A coefficient, as the level population and physical conditions can be complicated. These recommendations for line identification are recorded as 1 in the column `Validity`. These suggested identifications should be used with caution.

We show two examples of double Gaussian fitting in Figure 5. In the top panel, we fit partially blended CO and [CI] emission lines, and in the bottom panel, strongly blended OH and H₂O. In the first case, the fitting algorithm successfully resolved the blended lines. In the second case, the OH line was too weak to be detected, so the SNR is set to zero.

In some cases, we identified three possible line candidates. We did not fit any triple Gaussian profiles due to the complexity of the fit.

5.5 Noise Estimation

The problem of the noise estimation is two-fold. An accurate evaluation of the uncertainties of the fitted parameters needs reliable uncertainties for each spectral data point. However, no uncertainties are provided for the SPIRE data, and those supplied for PACS are unrealistic. Therefore, the uncertainties of the spectral data points need to be estimated from the spectrum itself. After the baseline fitting, the fitting process proceeds in two ways, one for full SED scans and one for short scans.

For sources with full SED scan, we feed the fitting routine with the spectra three times, two for getting a precise measurement of the uncertainties from the fluctuations of the baseline (hereafter baseline noise) and one for applying the baseline noise as the uncertainties of the spectral data points to get an accurate evaluation of the uncertainties of fitted parameters. For the short scan sources, there is only a single fitting process to get the estimation of the baseline noise because the continuum cannot be approximated precisely. Therefore, the baseline noise could be mixed with nearby strong lines. The baseline noise is fed to another fitting process to get the fitted parameters. The fits with all three fitting processes are labeled as “Global”, while the ones with only two fitting processes are labeled as “Local” in the `full_source_list.txt` file (see Section 5.6).

During the first pass through the data, the SNR of the line flux is calculated by taking the line strength divided by the standard deviation of the modified baseline times the FWHM of the line and 1.064 for a Gaussian profile (Equation 1). The modified baseline is a smaller baseline ranging over ± 5 spectral resolution elements with respect to the line centroid. This modification is designed for including enough wavelength channels into the baseline as well as avoiding the contamination from nearby strong lines. It is a rough estimation, which will not be used if the spectrum is good enough for the full noise estimation process, for the source that only has the first pass of fitting routine.

$$\text{SNR} = \frac{\text{line strength}}{1.064 \sigma_{\text{mod. baseline}} \times \text{FWHM}} \quad (1)$$

This first estimate occasionally yields anomalous uncertainties for blended lines or lines with other nearby lines, as the residual after subtracting the fitted line is not only the noise but also possibly not-yet-fitted emission lines. Thus in the second pass of the data, we

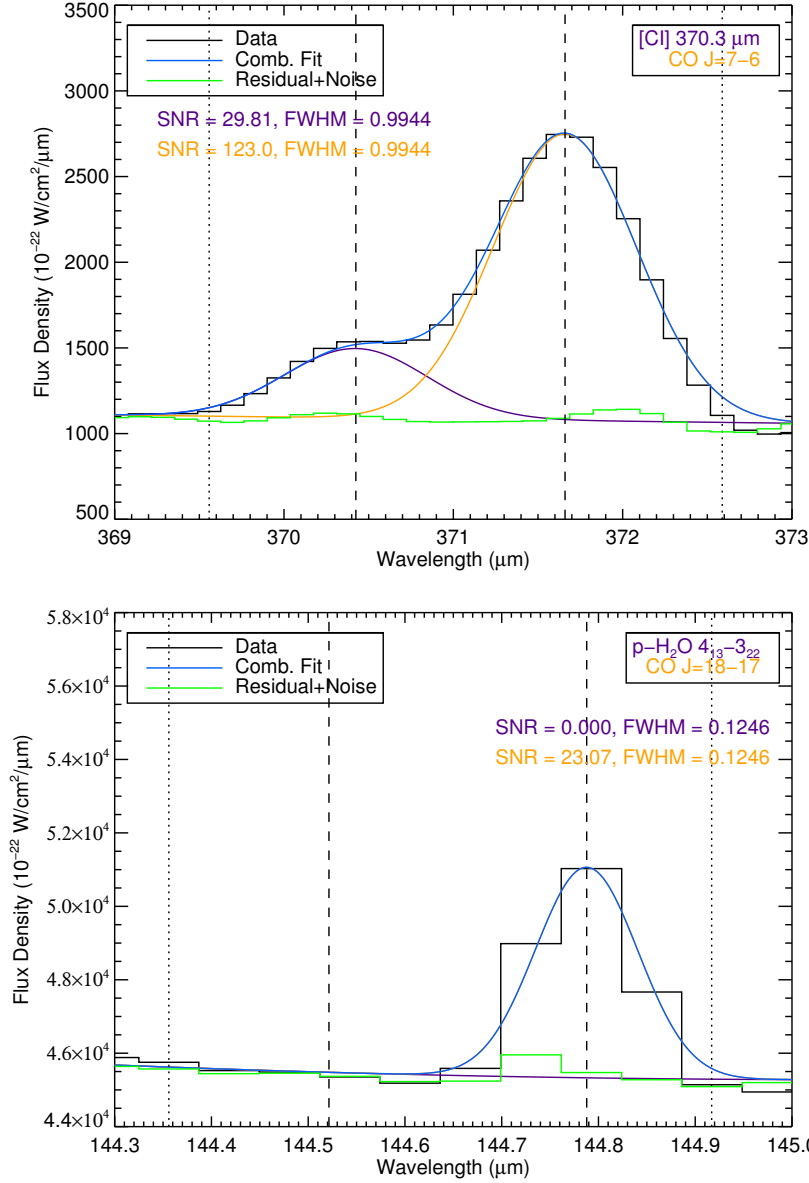


FIGURE 5: Examples of double-gaussian fitting. **Top:** For the blended [CI] $^3P_2 - ^3P_1$ line and the $^{12}\text{CO } J = 7 - 6$ line, for GSS30-IRS1, using fixed line centroids and FWHM constraints. The lines plotted are data (black), combined fit (blue), [CI] fit (purple), CO fit (yellow), and residual+noise (green) (See Section 5.5). The SNR of the [CI] and CO lines are 31.7 and 131, respectively. Both lines are considered as detections. **Bottom:** An example of a double fit in which only a single component was detected, for BHR71. We show the blended CO $J = 18 \rightarrow 17$ and p-H₂O $4_{13} - 3_{22}$ lines, for BHR71, using fixed line centroids and FWHM constraints. The color code is the same as the top figure. The SNR of the CO line is 23.07 and is significant; the water detection is not significant, so the SNR is set to zero.

subtract all lines identified with $\text{SNR} > 2$ (SNR calculated from the noise biased by not-yet-fitted lines) from the whole spectrum for each source. Then we use a top-hat smoothing function to approximate the continuum, which is released as a separate data product in the archive. This is the best product for modeling dust continuum emission (see next paragraph). We then subtract the continuum and produce a “flat” spectrum with continuum removed (Figure 7). From this procedure, a noise-only spectrum is retrieved. A second line fitting is then performed, exactly the same as the first pass, except that we use the noise-only spectrum to estimate the noise around each line. Furthermore, we replaced the noise-only spectrum under the line as the residual of the second fitting to improve the quality of the fitting. The noise-only spectrum is then replaced by the residual/noise-only spectrum. In the region where the individual line fitting is being performed, the uncertainties of the data points are set to those from the residual/noise-only spectrum, reflecting the typical baseline fluctuations near the line.

With the uncertainties of the data points in hand, a third line fitting is executed with the uncertainties we just measured. The smoothing function and continuum subtraction are also applied in the end of the third fitting. The SNRs are calculated from the residual/noise-only spectra from the third fitting. The fitting results produced from the third fitting, as well as the continuum and flat spectra, are those reported in the archive. By feeding in realistic uncertainties of the spectra, we can calculate reasonable uncertainties in the fitted parameters of the line. In Figure 6, we show the relation between the two different uncertainties, the uncertainty from the baseline and the uncertainty in the fitted line flux. Most points correlate well with the line of equality for both PACS and SPIRE spectra verifying that the uncertainties are correctly processed in the fitting routine.

While the uncertainties correlate well with the line of equality, there are some interesting features. In both figures, the points spread over about two orders of magnitude, partly reflecting the higher noise in some modules (see Figure 2 for example) and partly due to the changing FWHM in wavelength space, especially for SPIRE. In PACS, a bimodal distribution is found at low noise values. When the SNR is high (red points in Figure 6), normally the line profiles are well constrained, resulting in a similar uncertainty to the noise of the baseline. But there are some extra uncertainties for the fitted parameters due to the shape of the line, instrumental resolution, etc., which can cause larger errors in the fit for lines of low SNR. For strong lines ($\text{SNR} > 10$, red), those extra uncertainties are less significant, therefore the uncertainties cluster around the line of equality tightly. A bimodal population is not clearly seen in SPIRE fit uncertainties, but the strong lines are also better correlated with the line of equality. Finally, there is a spray of fits that lie above the line of equality reflecting the fact the the assumed line profile is not always a good fit to the data. These are dominated by low SNR lines for low noise and high SNR lines for high noise. Statistically speaking, the extra two steps in the line fitting routine increase the SNR 23% (38% for strong lines).

5.6 Reporting of Line-fitting Results

The results from the fitting routine are written in the folder `advanced_products`. The results include information on the fitted line parameters, as well as the flat spectrum and

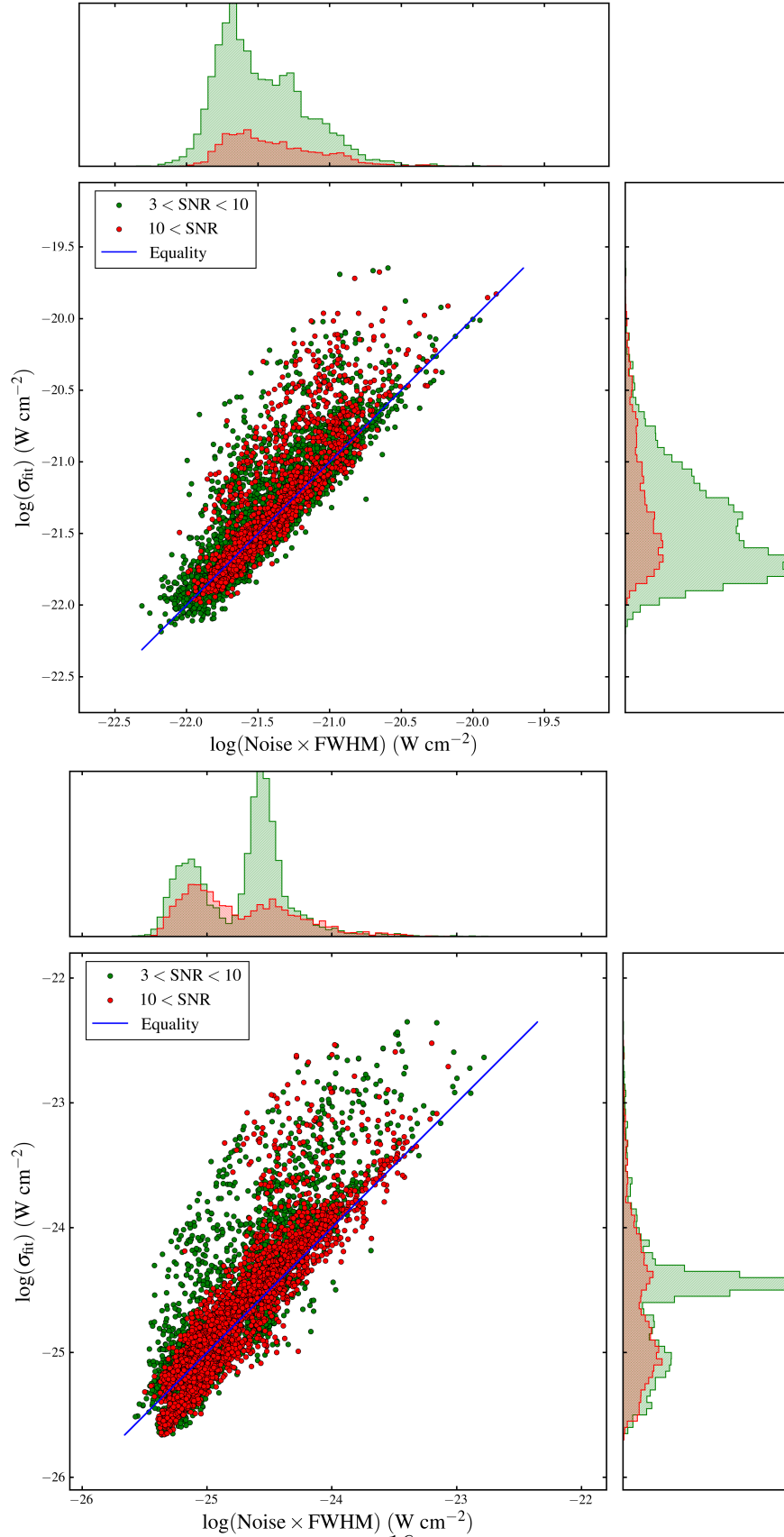


FIGURE 6: The correlations of the uncertainties measured from the baseline and the uncertainties of the fitted parameters (Top: PACS, Bottom: SPIRE). Detections with $3 < \text{SNR} < 10$ are plotted in green, while detections with $\text{SNR} > 10$ are plotted in red. The blue line indicates the equality of two quantities with zero offset.

pure continuum spectrum (Figure 7). Guidelines for properly interpreting the report are discussed below.

These text files are named `object_reduction_trim_lines.txt`, and they contain all of the information necessary to reconstruct the line fits. These ASCII table files contain either 17 or 18 columns (for the 1D spectrum or the spectrum of a single spaxel, respectively). The name and a short description of each column are listed in Table 2.

There are some caveats that should be considered before applying the results. Note that every line checked for a fit is listed, so many will be non-detections. Selecting on a suitable minimum SNR would be necessary to select likely detections. Then further quality control checks should be applied. First, the “Validity” column should be 1 for each unique plausible line detection. If an uncertainty column indicates -999 , the fit was unsuccessful and the fitted parameter and its uncertainty value should not be used; all lines flagged with -999 should be discarded. The -999 flag is applied to the columns of `Sig_Cen_WL(um)` and `Sig_FWHM(um)` if the quality of the fit is poor. This flag indicates that the line profile reached the local χ^2 minimum by moving to the edge of the allowed parameter space, stopping only due to imposed fitting constraints. In this case, the fitting routine is probably not identifying the input emission line. We do not recommend using any line flagged as 0 in `Validity` or -999 in other columns.

If an uncertainty column is flagged as -998 , the fitted parameters can be used, but the uncertainties will need to be extrapolated from other nearby line fits. The -998 flag appears only in the uncertainty columns `Sig_FWHM(um)`, `Sig_Cen_WL(um)` and `Sig_Str(W/cm2)`, and only if the line width is fixed to a particular value (the instrumental resolution at that wavelength). In this case uncertainties cannot be generated, but the fitted parameters are considered reliable. We fix most line widths in PACS line fits (an exception is [O I] $63 \mu\text{m}$, which has been observed to be broader than the instrumental line width), but only fix the width for cases of double-Gaussian fitting in SPIRE line fits. In these cases of fixed line width, we cannot calculate uncertainties for the line width. If an uncertainty is needed, we recommend using values for a nearby line if available. An example of part of the fitting results table is shown in Table 3.

A summary of sources and how they were processed can be found at “`full_source_list_refine.txt`”. It lists the names of the processed sources in order and the status of access to different reductions. Additional information can be found at “`full_source_list.txt`”, which includes the information about the noise re-estimation (see Section 5.5).

In total, we performed line fitting on 67 and 33 objects in the PACS and SPIRE bands, respectively. 2-D PACS datacubes consist of four modules of 25 spaxels each, and SPIRE datacubes consist of two modules of 33 and 19 spaxels. Including all spaxels in the 2-D datacube, totaling 264590 PACS and 60330 SPIRE line fitting processes, we found 9626 and 9801 detections without any anomaly in PACS and SPIRE fits, compared to 254964 and 50529 non-detections, including anomalies (fits with $\text{SNR} > 3$ but a flag for poor fitting quality applied). Any line fit in which an unphysical broad component was fitted, the line centroid diverged and reached our pre-defined boundary, or the fitted line are blended

with another line with lower Einstein-A value, was determined to be an anomaly. There were a total of 890 and 9922 anomalies with detection in the PACS and SPIRE fits. On average, we found 143.67 and 297 lines per object in PACS and SPIRE bands. The fitting results of all PACS and SPIRE sources are also stored in four ASCII files for 1-D and 2-D spectra (“CDF_archive_pacs[spire]_1d[cube]_lines.txt”). The users may find these summary tables useful.

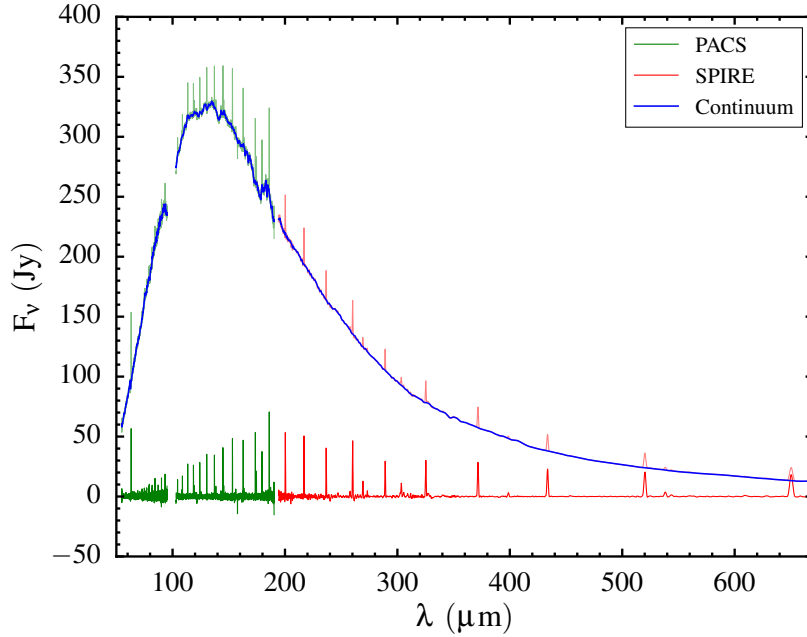


FIGURE 7: The spectrum of BHR71 with flat spectrum (green/red for PACS/SPIRE, respectively) and continuum (blue) overplotted. The continuum is the result of the smoothing function applied to the line-subtracted spectrum. The flat spectrum is produced by removing the continuum from the original spectrum. The comparison of the continuum and the flat spectrum at the edge of the PACS band shows that the fitting algorithm works well even in the region with severe instrumental effects. The SPIRE spectrum is scaled by 0.6 in order to match the PACS flux.

TABLE 2: Description of each column in the line information table

Column name	Unit	Description
Lines	...	The species and the transition of the line
LabWL (um) ^a	μm	The theoretical or laboratory wavelength of the transition.
ObsWL (um)	μm	The fitted wavelength of the transition.
Sig_Cen (um)	μm	The uncertainty of the fitted wavelength.
Str (W/cm2) ^c	W cm^{-2}	The integrated line strength calculated from the fitted Gaussian profile.
Sig_Str (W/cm2) ^c	W cm^{-2}	The uncertainty of the integrated line strength.
FWHM (um)	μm	The full width at half maximum of the fitted Gaussian profile.
Sig_FWHM (um)	μm	The uncertainty of the full width at half maximum.
Base (W/cm2/um) ^c	$\text{W cm}^{-2} \mu\text{m}^{-1}$	The specific flux of the fitted continuum at the line centroid.
Noise (W/cm2/um) ^c	$\text{W cm}^{-2} \mu\text{m}^{-1}$	The noise level calculated from the residual of second fitting and the line subtraction procedure. (See Section 5.5)
SNR	...	The signal-to-noise ratio of the fitted line strength.
E_u (K) ^a	K	The energy of the upper level of the transition.
A (s-1) ^a	1/s	The Einstein-A value of the transition.
g ^a	...	The multiplicity of the upper level of the transition.
RA (deg)	°	The Right Ascension of the object or spaxel.
Dec (deg)	°	The Declination of the object or spaxel.
Pixel_No. ^b	...	The spaxel number or name at PACS and SPIRE module. In PACS, they are labeled numerically, while specific names are assigned in SPIRE module.
Blend	...	The status of blended lines. Red means that this line is blended with another component at longer wavelength; Blue means that this line is blended with another component at shorter wavelength; Red/Blue means that this line is blended at both side of the line profile. More details in Section 5.4.
Validity	...	The overall suggestion whether to use this fitted line profile based on the fitting quality and blending criteria. More details in Section 5.4.

^a The theoretical information of each transition is acquired from Leiden Atomic and Molecular Database (LAMDA)(Schöier et al., 2005).

^b This column is not shown in the 1D spectra line fitting results.

^c This unit is in intensity unit (per arcsec²) for the fitting result of each spaxel in SPIRE.

TABLE 3: A part of the table with 1-D spectrum fitting results for BHR71. The tables in the ASCII files have the same columns and style except that the rows are chopped into three parts here for better display. Also this table has selected lines from different parts of the original results to demonstrate different flags, etc. As we mentioned in Section 5.6, any column with -999 means that this fitting result is not well-constrained. Therefore, the Validity flag is set to be 0.

Line	LabWL (um)	ObsWL (um)	Sig_Cen (um)	Str (W/cm2)	Sig_str (W/cm2)
CO48-47	54.98621750	54.98061538	0.02927984522	-3.549060753e-21	4.437289787e-21
CO47-46	56.12189865	56.10322339	0.01831864637	-2.522146694e-21	1.968213046e-21
p-H2O4_31-3-22	56.32640076	56.30469125	0.005550669531	8.546860028e-21	2.018027526e-21
CO46-45	57.30772781	57.30684852	0.07258929923	-6.175549719e-22	1.905239186e-21
o-H2O6_61-6-52	63.91602325	63.91900274	0.02849165434	1.607089659e-21	1.936054194e-21
o-H2O7_61-7-52	63.95696259	63.93649292	-999.0000000	9.094273736e-22	1.944308634e-21
CO29-28	90.16526794	90.15535779	0.001488817819	2.516335920e-20	1.724530999e-21
p-H2O9_37-8-44	118.4082565	118.4082565	-998.0000000	1.293496266e-22	3.590390570e-21
CO22-21	118.5837021	118.5837021	-998.0000000	7.102478570e-20	3.600906591e-21
p-H2O8_35-8-26	148.7115631	148.7528381	-999.0000000	-4.994561563e-21	1.336922291e-21
FWHM (um)	Sig_FWHM (um)	Base (W/cm2/um)	Noise (W/cm2/um)	SNR	E_u (K)
0.03897858372	-998.0000000	5.959023714e-18	1.609286205e-19	0.5317560724	6457.230000
0.03905097576	-998.0000000	6.165975858e-18	6.017235690e-20	1.008787745	6195.570000
0.03906316840	-998.0000000	6.191619649e-18	6.555463955e-20	3.136852224	552.3000000
0.03912018226	-998.0000000	6.333289054e-18	7.985864874e-20	0.1857852210	5939.210000
0.03936703190	-998.0000000	7.409176833e-18	6.024669684e-20	0.6368432667	1503.600000
0.03936783131	-998.0000000	7.412447305e-18	6.114173180e-20	0.3550971309	1749.900000
0.03616096086	-998.0000000	8.550760327e-18	6.351713920e-20	10.29665339	2399.820000
0.1169993003	-998.0000000	6.793961540e-18	2.734176619e-20	0.03800263561	1749.900000
0.1169993003	-998.0000000	6.778255746e-18	2.734176619e-20	20.86692572	1397.380000
0.1251977122	-998.0000000	4.255336709e-18	1.723847688e-20	2.175005976	1511.000000
A (s-1)	g	RA (deg)	Dec (deg)	Blend	Validity
0.006556000000	97	180.3985138	-65.14783478	x	1
0.006326000000	95	180.3985138	-65.14783478	x	1
1.452000000	9	180.3985138	-65.14783478	x	1
0.006091000000	93	180.3985138	-65.14783478	x	1
0.3533000000	39	180.3985138	-65.14783478	Red/Blue	1
0.5828000000	45	180.3985138	-65.14783478	Red/Blue	0
0.002126000000	59	180.3985138	-65.14783478	x	1
0.01724000000	19	180.3985138	-65.14783478	DoubleGaussian	1
0.001006000000	45	180.3985138	-65.14783478	DoubleGaussian	1
0.1235000000	17	180.3985138	-65.14783478	Red	0

5.7 Contour Plots

To further visualize the fitting results, we produced contour plots of each line (line contours) overplotted on the local continuum at the wavelength of the line centroid (e.g., Figure 8). The contours are the minimum curvature surface interpolated from lines with SNR greater than 3. The adjacent contours are in steps of 20% of the peak, and the lowest contour (20% of the peak) is not shown in the plots. The crosses in each figure indicate the physical position of each spaxel and the center cross indicates the pointing position. The crosses marked in green indicate spaxels with significant line detections; the user can judge the reliability of detailed structure in an individual contour plot based on the detections. We plot contours only for maps with detections in *more* than 2 spaxels.

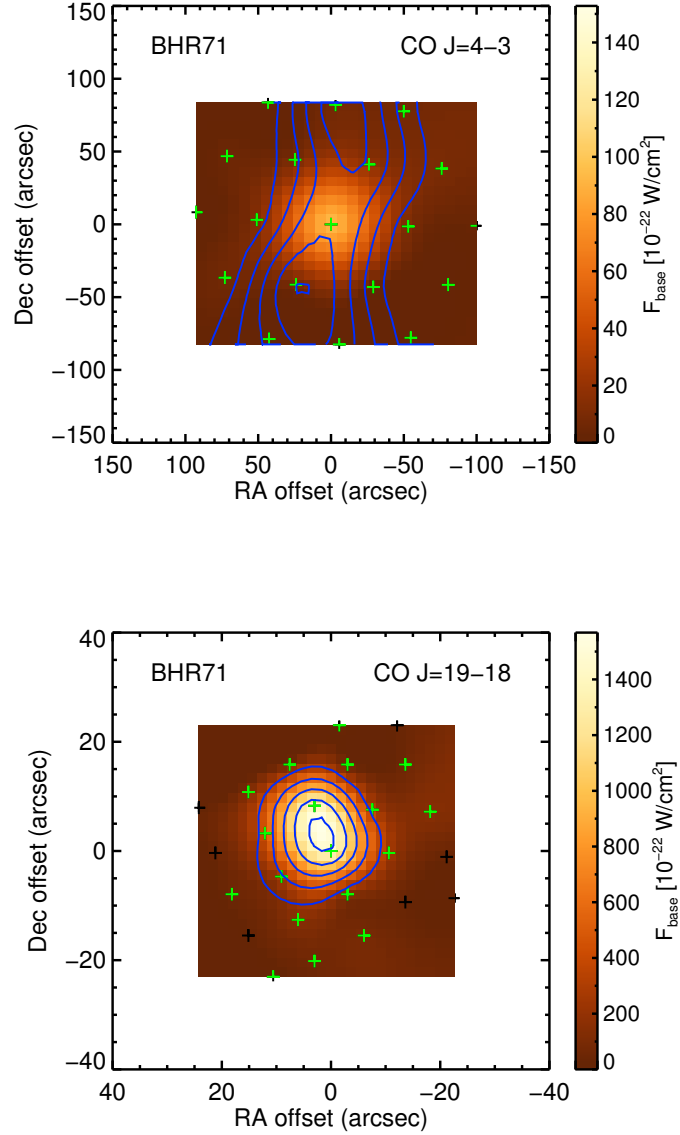


FIGURE 8: An example of 2-D EPS contour maps of BHR71 $^{12}\text{CO J} = 4 - 3$ and $^{12}\text{CO J} = 19 - 18$ line emission (blue contours) vs. local continuum (filled background) observed in SPIRE and PACS respectively (Yang et al., in prep.) The green crosses indicate the spaxels that have detections.

6 Archive Structure and File Format

The file and directory trees contained in the archive are indicated in Figure 9. We provide the high-level data from the optimized pipeline and the products of line fitting results. The following section describes the file structure and how to interpret the individual formats.

6.1 File Structure

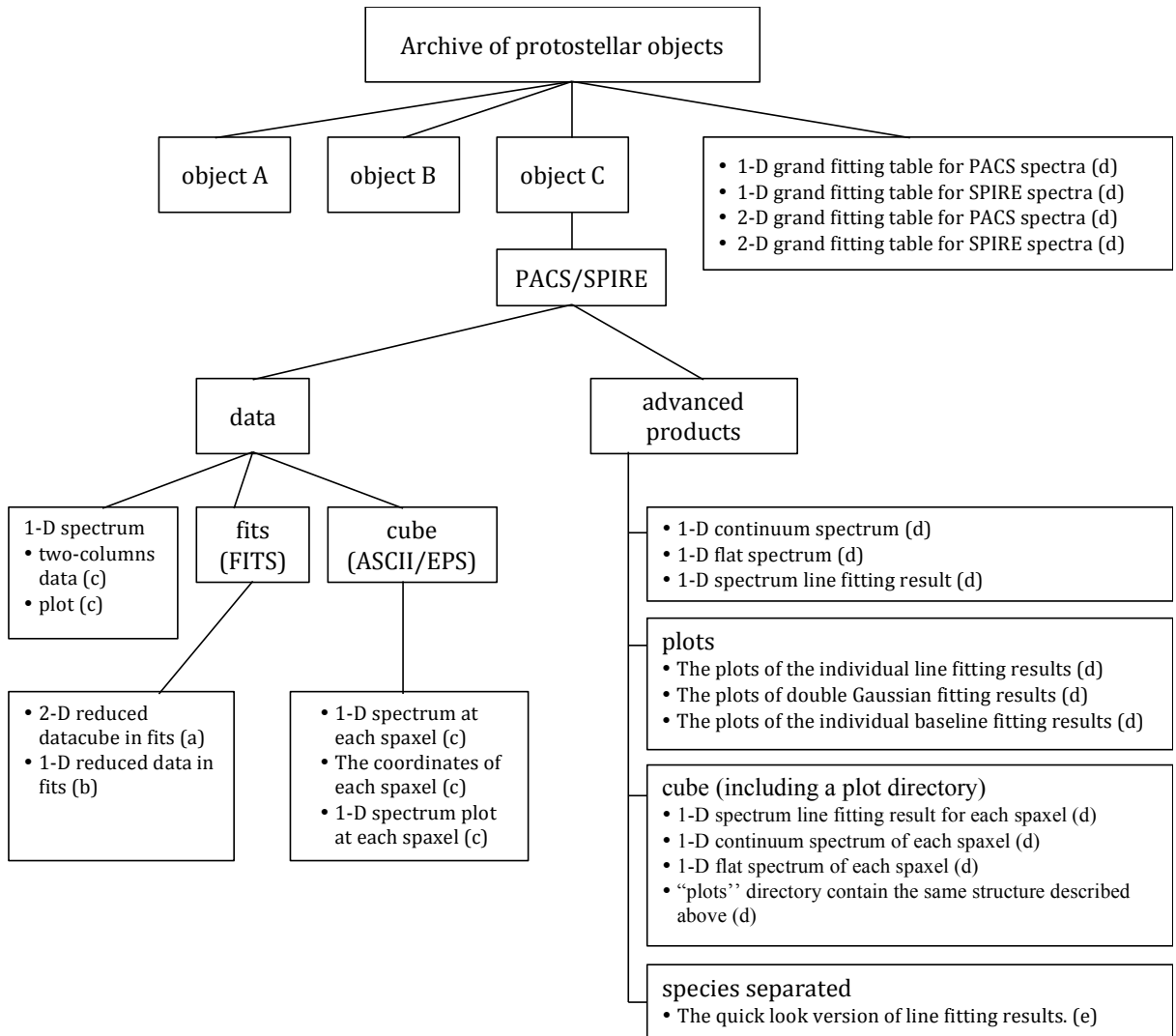


FIGURE 9: The hierarchy structure of the archival file system. Files are organized primarily by the targets, and every target directory has the same substructure. The PACS and SPIRE high-level data and fitting results are stored in separate directories with the same structure.

The schematic view of the file structure is shown in Figure 9. If there is no PACS or SPIRE observation available for a target, then the corresponding directory is not present.

The detailed description of each product is described below. The products are identified in Figure 9 with the same letter (a through e) used to identify the following sections.

6.2 File Format

(a) 2-D reduced datacubes (FITS)

- PACS

We generate three datacubes for PACS in FITS format: Source – Nod A; Source – Nod B; Average (Source – (Nod A + Nod B) / 2). These can be read as dataplanes for each spaxel, with appropriate RA/Dec, and flux vs. wavelength. They are generated with wavelength grid oversample = 2 and upsample = 1 by default. These cubes include all corrections (in particular jitter removal). The

Filename:

```
OBSID_1342xxxxxx_Targetname_blue/red_rebinnedcubesnoda_os#sf#.fits  
OBSID_1342xxxxxx_Targetname_blue/red_rebinnedcubesnodb_os#sf#.fits  
OBSID_1342xxxxxx_Targetname_blue/red_finalcubes_os#sf#.fits
```

We also generate these same three cubes WITHOUT the pointing offset correction, with the addition of “_nojitter.fits” to the filename. We include the offset-corrected product only if the correction was successful. We include the non-offset corrected version for *all* sources. *If a jitter-corrected version is supplied, it means that we recommend using it.*

- SPIRE

We generate one datacube for SPIRE in FITS format. These can be read as dataplanes for each spaxel, with appropriate RA/Dec, and flux vs. wavelength. Note that both SLW and SSW modules are included in a single FITS file, therefore . These cubes include all corrections.

Filename:

```
1342xxxxxx_spectrum_extended_HR_aNB_15.fits
```

There is no offset-corrected product being generated for SPIRE data.

(b) 1-D reduced spectra (FITS)

- PACS

We generate FITS files for three cases, each with and without jitter correction; all six resulting files have the point source (PSF) correction applied. We also provide files in ASCII and EPS formats (see next section).

Filename:

```
OBSID_1342xxxxxx_Targetname_blue/red_centralSpaxel_  
PointSourceCorrected_Corrected3x3NO_slice00_os#sf#.fits
```

This is the simplest product, which is just the spectrum of the central spaxel with only the PSF correction applied. The “slice” is only non-zero for multiple ranges-can or linescan observations, representing different wavelength settings within the original OBSID.

Filename:

```
OBSID_1342xxxxxx_Targetname_blue/red_centralSpaxel_
PointSourceCorrected_Corrected3x3YES_slice00_os#sf#.fits
```

This is the same as the above product but with the jitter/pointing correction for the loss of light in between pixels included in addition to the PSF correction. That is, we start with the central spaxel, and apply both the PSF and pointing/jitter correction.

We also generate the straight sum of the 3x3 spaxels, including PSF and pointing/jitter corrections:

Filename:

```
OBSID_1342xxxxxx_Targetname_blue/red_central9Spaxels_
PointSourceCorrected_slice00_os#sf#.fits
```

A summation of the central 9 spaxels (the “3x3” case) with PSF correction applied.

So in summary, all three files have the point source (PSF) correction applied. The “3x3NO” is just this raw product. The “3x3YES” is the flux of the central spaxel after correcting for the PSF and the pointing/jitter. The “central9Spaxels” is the sum of the flux in the central 3x3 spaxels, still including the PSF/pointing jitter corrections.

We also output a version of these files without the pointing/jitter corrections. The filename is similar to the previous version, but with “_nojitter.fits” appended; “nojitter” refers to no jitter corrections applied.

We compare the three products for the case of TMR1 in Figure 10. The green spectrum shows the centralSpaxel product without the absolute flux calibration of the 3x3 aperture extraction; the red spectrum is the straight sum of the central 3x3 spaxels, and the black spectrum is the best product, combining the SNR of the central spaxel with the absolute flux calibration of the 3x3 aperture extraction.

- SPIRE

We generate one FITS file containing the SPIRE 1-D spectrum for each target. The spectra are processed by the pipeline setting described in Section 4.2 including “SemiExtendedSourceCorrector” correction.

Filename:

```
Targetname_spire_corrected.fits
```

In this FITS file, it still contains all of the dataplanes with the same order as the 2-D datacube. But only the planes 5 and 8 containing the central spaxel in SLW

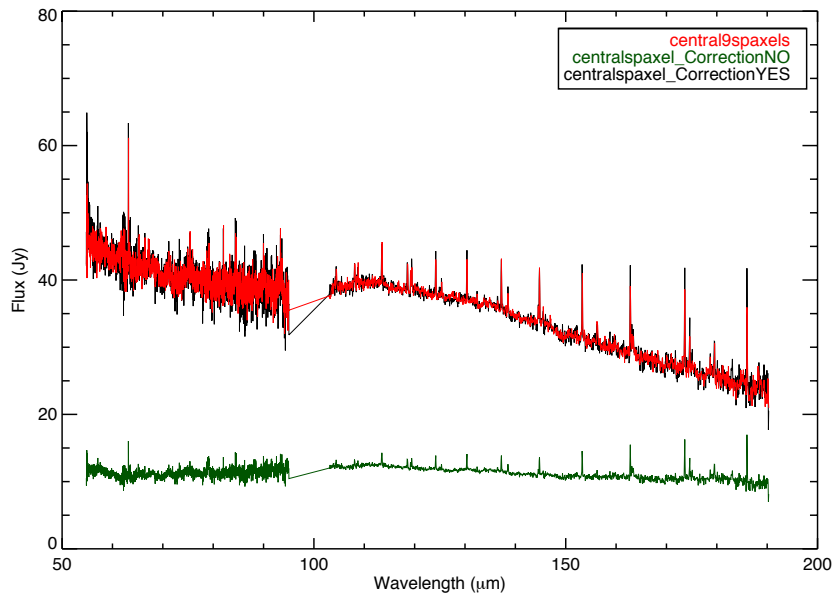


FIGURE 10: Plot of our three PACS pipeline products, for protostar TMR1. The green spectrum shows the central spaxel product, with best SNR without accounting for source extent. The red spectrum is the sum of the central 9 spaxels in the PACS array; this likely includes all of the source flux, but also added noise from low SNR spaxels. The black spectrum is the best compromise product, flux calibrated to the red spectrum that has most of the source flux, but with SNR consistent with the green spectrum. Note that lines are stronger in black than red with only modest increase of noise, therefore higher SNR.

and SSW are the ones with correct values. The lines are fitted from these spectra as well.

(c) 1-D reduced spectra (two-columns ASCII/EPS)

For both 1-D reduced spectra and 2-D datacube, we extract the information (wavelength and flux) from the FITS files and report them into two-column ASCII format with plots of the corresponding spectrum for each spaxel or source. The same plotting method is applied to both 1-D spectra and spaxels in datacube. In PACS, we put all of the modules together in ASCII files and plots, including B2A, B2B, and R1. In addition, because the pointing coordinate of each spaxel varied slightly with wavelength, we report the files ending with “coord” containing the coordinates (RA/Dec) of each spaxel at each wavelength point. The coordinates reported in 1-D spectra fitting results table are derived from the mean values of the coordinates across all wavelengths. The standard deviations of the coordinates across all wavelengths range from from 0.0073'' to 0.607'' for RA, and 0.0233'' to 0.4386'' for Dec. The mean values of the standard deviation are 0.166'' and 0.0675'' in RA and Dec respectively. But different modules are reported separately for SPIRE due to their different spaxel configurations. **We recommend users to use the coordinates from the files we provided instead of reading in from the header of the FITS files.**

Filename:

(1-D)

Targetname_reduction_trim.txt

Targetname_reduction_trim.eps

(2-D)

Targetname_pacs_pixel##_os#sf#.txt

Targetname_pacs_pixel##_os#sf#_coord.txt

Targetname_pacs_pixel##_os#sf#.eps

Targetname_pixelname.txt

Targetname_pixelname.eps

These ASCII files (and the EPS plots generated alongside them) are trimmed consistently at specific wavelengths. Here we described trimming details for PACS and SPIRE separately.

- PACS

For the shortest wavelength module (B2A), we remove all wavelengths short of 54.80 μm , and long of 72.3 μm . For the next shortest (B2B), we trim all wavelengths short of 72.3 μm and long of 95.05 μm . For the third (R1; 100-145 μm), we remove all wavelengths short of 101.4 μm and long of 143.0 μm . For the fourth (R1; 145-210 μm), we trim all wavelengths short of 190.31 μm , and long of 143.0 μm .

- SPIRE

For the shorter wavelength module (SSW), we remove all wavelengths short of 195 μm , and long of 304 μm . For the longer wavelength module (SLW), we remove all wavelengths short of 304 μm .

We find this method gives the best overall continuum fit between modules, with the highest SNR and consistent continuum in the overlap regions, stitched into single 1-D spectrum. The FITS files previously described do not use these trim points and present the full spectra with the overlap regions included twice. An example of the final merged spectra of the protostar TMR1 (PACS and SPIRE) are shown in Figure 11, with each module highlighted by color.

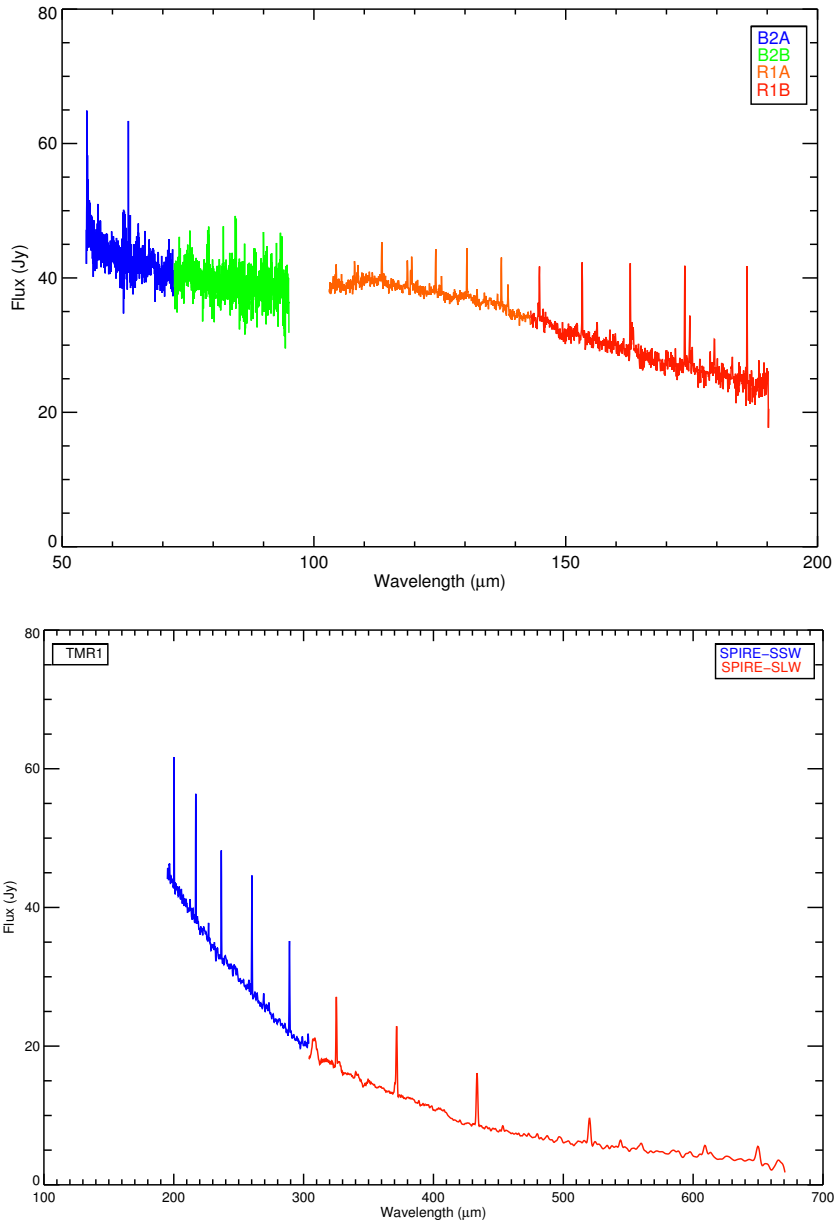


FIGURE 11: **Top:** An example 1-D PACS spectrum of TMR1, with the four modules highlighted by color. **Bottom:** An example 1-D SPIRE spectrum of TMR1, with the two modules highlighted by color.

- (d) Line fitting results The line fitting results are reported in text and figures format. The ASCII files provide the tables of the fitting results so that users can read them in with any language they prefer. The figures visualize the fitting results with the original data, fitted line(s), and residual. The users can visually check the fitting results with the figures easily.

Filename:

(PACS)

```
Targetname_reduction_trim_lines.txt
Targetname_reduction_trim_continuum.txt
Targetname_reduction_trim_flat_spectrum.txt
Targetname_pacs_pixel##_os#sf#_lines.txt
Targetname_pacs_pixel##_os#sf#_continuum.txt
Targetname_pacs_pixel##_os#sf#_flat_spectrum.txt
```

(SPIRE)

```
Targetname_spire_corrected_lines.txt
Targetname_spire_corrected_continuum.txt
Targetname_spire_corrected_flat_spectrum.txt
Targetname_pixelname_lines.txt
Targetname_pixelname_continuum.txt
Targetname_pixelname_flat_spectrum.txt
```

The ASCII format line fitting results are presented in three output forms (lines, continuum, and flat_spectrum), as listed above in the first two blocks of file names. The first contains the full report of the line fitting results using the method described in Section 5, containing the fitted line parameters (Table 2) of each line in the full input list – including non-detections. Users can simply read this report and apply the fitting results. The second file contains the continuum spectrum of the source produced by subtracting the fitted lines from the original spectrum. The third file is the counterpart of the continuum file, a continuum-subtracted spectrum in which only the fitted lines and flat baseline remain (Figure 7). The file names of PACS spectra are listed in the first block with the first three as the products of 1-D spectra and last three as the products of 2-D spectra, while file names of SPIRE spectra are listed in the second block with the same fashion.

(Fitting table including all sources)

```
CDF_archive_pacs_1d_lines.txt
CDF_archive_pacs_cube_lines.txt
CDF_archive_spire_1d_lines.txt
CDF_archive_spire_cube_lines.txt
```

The fitting results of 1-D PACS, 1-D SPIRE, 2-D PACS, and 2-D SPIRE of all sources are stored into separate ASCII files with similar tables to those described above and in Section 5 with an additional column with the object name.

(Individual line fitting plot in PACS)

Targetname_spectrum_line_subtracted_reduction_trim.eps

Targetname_reduction_trim_linename.eps

Targetname_reduction_trim_line1+line2.eps

(Individual line fitting plot in SPIRE)

Targetname_spectrum_line_subtracted_spire_corrected.eps

Targetname_spire_corrected_linename.eps

Targetname_spire_corrected_line1+line2.eps

The figures are all presented in typical spectra with various levels of data, as listed above. The first three in the six items are figures for PACS, while the last three of six are for SPIRE. The ones with “spectrum_line_subtracted” provide overviews for line fitting results of each object and each instrument. It includes the original data (black), continuum (blue), and flat spectrum (green). The ones with “linename” provide the visualization of the fitting result for each line (Figure 12 top). It includes original data (black), fitted line (blue), and residual/noise (green). The vertical lines represent the allowed region for line (dash line) and the region taken for the baseline fitting (dotted line). And the SNR and FWHM are printed within the figures. The fitting results of the double Gaussian are plotted in figures with two lines in their file names (“line1+line2”) with an additional fitted line in orange (Figure 5). We also report the fitting results of the baseline in the subdirectory named “base” (Figure 12 bottom). The plot includes the original data (black), the fitted baseline (purple), residual (red), and the points taken in the baseline fitting (asterisks). There is another directory named “cannot_fit” which includes the very rare case when the fitting failed to coverage.

(e) Quick look output for the fitting results

Filename:

Targetname_reduction_trim_lines_species.txt

Targetname_spire_corrected_species.txt

This output provides the user a convenient quick look at the source spectral properties and evaluation of the fitting quality. These files contain the sorted line information of either the 1-D spectrum or the spectrum of each spaxel for given molecular/atomic species. The line profiles of seven different species are separated including ^{12}CO , ^{13}CO , HCO^+ , OH , $\text{o-H}_2\text{O}$, $\text{p-H}_2\text{O}$, and atomic fine-structure transitions. The data of each molecule are stored in the corresponding directories.

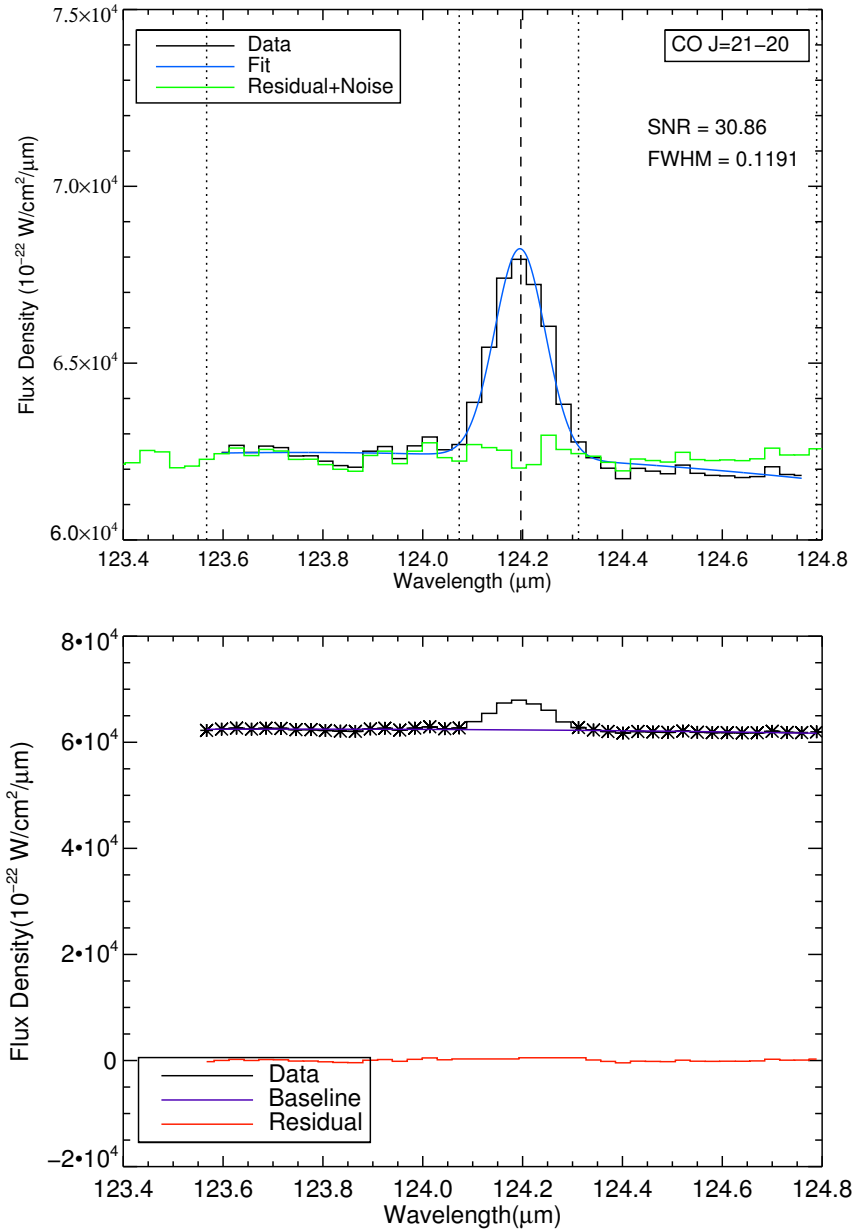


FIGURE 12: **Top:** An example of single line fitting result of ^{12}CO J = 21 – 20 in BHR71. **Bottom:** An example of the baseline fitting result at the region of ^{12}CO J = 21 – 20 in BHR71. The asterisks indicate the points being taken into the baseline fitting.

7 Sourcelist and Data Product Status

The comprehensive source list, OBSID number, RA, Dec, and reduction type are listed in [Table 10](#).

TABLE 4: Line list for single Gaussian fitting: o-H₂O

Wavelength (μm)	Line name	Wavelength (μm)	Line name
55.13238	o-H ₂ O 8 ₂₇ – 7 ₁₆	55.84108	o-H ₂ O 10 ₂₉ – 10 ₁₁₀
56.81777	o-H ₂ O 9 ₀₉ – 8 ₁₈	57.39511	o-H ₂ O 7 ₅₂ – 8 ₂₇
58.70051	o-H ₂ O 4 ₃₂ – 3 ₂₁	61.31782	o-H ₂ O 5 ₄₁ – 6 ₁₆
62.92979	o-H ₂ O 9 ₁₈ – 9 ₀₉	63.32514	o-H ₂ O 8 ₁₈ – 7 ₀₇
63.91602	o-H ₂ O 6 ₆₁ – 6 ₅₂	63.95796	o-H ₂ O 7 ₆₁ – 7 ₅₂
65.16779	o-H ₂ O 6 ₂₅ – 5 ₁₄	66.09434	o-H ₂ O 7 ₁₆ – 6 ₂₅
66.43937	o-H ₂ O 3 ₃₀ – 2 ₂₁	67.27067	o-H ₂ O 3 ₃₀ – 3 ₀₃
70.70435	o-H ₂ O 8 ₂₇ – 8 ₁₈	71.94881	o-H ₂ O 7 ₀₇ – 6 ₁₆
74.94690	o-H ₂ O 7 ₂₅ – 6 ₃₄	75.38257	o-H ₂ O 3 ₂₁ – 2 ₁₂
75.49740	o-H ₂ O 8 ₅₄ – 8 ₄₅	75.83188	o-H ₂ O 6 ₅₂ – 6 ₄₃
75.91180	o-H ₂ O 5 ₅₀ – 5 ₄₁	77.76345	o-H ₂ O 7 ₅₂ – 7 ₄₃
78.74431	o-H ₂ O 4 ₂₃ – 3 ₁₂	81.40747	o-H ₂ O 9 ₂₇ – 9 ₁₈
82.03351	o-H ₂ O 6 ₁₆ – 5 ₀₅	82.97879	o-H ₂ O 8 ₃₆ – 8 ₂₇
84.76907	o-H ₂ O 7 ₁₆ – 7 ₀₇	85.77088	o-H ₂ O 8 ₄₅ – 8 ₃₆
92.81312	o-H ₂ O 6 ₄₃ – 6 ₃₄	94.64643	o-H ₂ O 6 ₂₅ – 6 ₁₆
94.70758	o-H ₂ O 4 ₄₁ – 4 ₃₂	104.09629	o-H ₂ O 6 ₃₄ – 6 ₂₅
108.07588	o-H ₂ O 2 ₂₁ – 1 ₁₀	112.51342	o-H ₂ O 7 ₄₃ – 7 ₃₄
112.80576	o-H ₂ O 4 ₄₁ – 5 ₁₄	113.54021	o-H ₂ O 4 ₁₄ – 3 ₀₃
114.45656	o-H ₂ O 9 ₂₇ – 10 ₁₁₀	116.35288	o-H ₂ O 8 ₃₆ – 9 ₀₉
116.78196	o-H ₂ O 7 ₃₄ – 6 ₄₃	121.72477	o-H ₂ O 4 ₃₂ – 4 ₂₃
123.46352	o-H ₂ O 9 ₃₆ – 9 ₂₇	127.88735	o-H ₂ O 7 ₂₅ – 7 ₁₆
129.34220	o-H ₂ O 9 ₄₅ – 9 ₃₆	132.41173	o-H ₂ O 4 ₂₃ – 4 ₁₄
133.55242	o-H ₂ O 8 ₃₆ – 7 ₄₃	134.93863	o-H ₂ O 5 ₁₄ – 5 ₀₅
136.49943	o-H ₂ O 3 ₃₀ – 3 ₂₁	156.26908	o-H ₂ O 5 ₂₃ – 4 ₃₂
159.05453	o-H ₂ O 8 ₄₅ – 7 ₅₂	159.40427	o-H ₂ O 6 ₃₄ – 7 ₀₇
160.51410	o-H ₂ O 5 ₃₂ – 5 ₂₃	166.81885	o-H ₂ O 7 ₃₄ – 7 ₂₅
174.63028	o-H ₂ O 3 ₀₃ – 2 ₁₂	174.92441	o-H ₂ O 4 ₃₂ – 5 ₀₅
179.53118	o-H ₂ O 2 ₁₂ – 1 ₀₁	180.49281	o-H ₂ O 2 ₂₁ – 2 ₁₂
187.81488	o-H ₂ O 8 ₅₄ – 9 ₂₇	212.53093	o-H ₂ O 5 ₂₃ – 5 ₁₄
226.76647	o-H ₂ O 6 ₂₅ – 5 ₃₂	229.21129	o-H ₂ O 8 ₄₅ – 9 ₁₈
231.25379	o-H ₂ O 8 ₂₇ – 7 ₃₄	234.53645	o-H ₂ O 7 ₄₃ – 6 ₅₂
256.59928	o-H ₂ O 8 ₅₄ – 7 ₆₁	257.80114	o-H ₂ O 3 ₂₁ – 3 ₁₂
258.82221	o-H ₂ O 6 ₃₄ – 5 ₄₁	259.98875	o-H ₂ O 3 ₁₂ – 2 ₂₁
261.46379	o-H ₂ O 7 ₂₅ – 8 ₁₈	273.19988	o-H ₂ O 3 ₁₂ – 3 ₀₃
483.00214	o-H ₂ O 5 ₃₂ – 4 ₄₁	538.30236	o-H ₂ O 1 ₁₀ – 1 ₀₁

TABLE 5: Line list for single Gaussian fitting: p-H₂O

Wavelength (μm)	Line name	Wavelength (μm)	Line name
55.85970	p-H ₂ O 6 ₅₁ – 7 ₂₆	55.98480	p-H ₂ O 7 ₇₁ – 7 ₆₂
56.02824	p-H ₂ O 10 ₁₉ – 10 ₀₁₀	56.32640	p-H ₂ O 4 ₃₁ – 3 ₂₂
56.77240	p-H ₂ O 9 ₁₉ – 8 ₀₈	57.63798	p-H ₂ O 4 ₂₂ – 3 ₁₃
57.71080	p-H ₂ O 8 ₁₇ – 7 ₂₆	58.37824	p-H ₂ O 6 ₄₂ – 7 ₁₇
59.98863	p-H ₂ O 7 ₂₆ – 6 ₁₅	60.16365	p-H ₂ O 8 ₂₆ – 7 ₃₅
60.23082	p-H ₂ O 7 ₆₂ – 8 ₃₅	61.81016	p-H ₂ O 4 ₃₁ – 4 ₀₄
61.91772	p-H ₂ O 4 ₄₀ – 5 ₁₅	62.43311	p-H ₂ O 9 ₂₈ – 9 ₁₉
63.45961	p-H ₂ O 8 ₀₈ – 7 ₁₇	63.88177	p-H ₂ O 7 ₆₂ – 7 ₅₃
67.09082	p-H ₂ O 3 ₃₁ – 2 ₂₀	71.06907	p-H ₂ O 5 ₂₄ – 4 ₁₃
71.54146	p-H ₂ O 7 ₁₇ – 6 ₀₆	71.78955	p-H ₂ O 5 ₅₁ – 6 ₂₄
72.03407	p-H ₂ O 8 ₁₇ – 8 ₀₈	73.61471	p-H ₂ O 9 ₃₇ – 9 ₂₈
75.78324	p-H ₂ O 5 ₅₁ – 5 ₄₂	75.81532	p-H ₂ O 7 ₅₃ – 7 ₄₄
76.42386	p-H ₂ O 6 ₅₁ – 6 ₄₂	78.93042	p-H ₂ O 6 ₁₅ – 5 ₂₄
80.22431	p-H ₂ O 9 ₄₆ – 9 ₃₇	80.55884	p-H ₂ O 8 ₅₃ – 8 ₄₄
81.21765	p-H ₂ O 7 ₂₆ – 7 ₁₇	81.69220	p-H ₂ O 8 ₃₅ – 7 ₄₄
83.28606	p-H ₂ O 6 ₀₆ – 5 ₁₅	89.99061	p-H ₂ O 3 ₂₂ – 2 ₁₁
90.05205	p-H ₂ O 7 ₄₄ – 7 ₃₅	94.21193	p-H ₂ O 5 ₄₂ – 5 ₃₃
103.91892	p-H ₂ O 6 ₄₂ – 6 ₃₃	103.94278	p-H ₂ O 6 ₁₅ – 6 ₀₆
111.63078	p-H ₂ O 5 ₂₄ – 5 ₁₅	113.95081	p-H ₂ O 5 ₃₃ – 5 ₂₄
117.68692	p-H ₂ O 9 ₄₆ – 8 ₅₃	118.40826	p-H ₂ O 9 ₃₇ – 8 ₄₄
122.52519	p-H ₂ O 8 ₄₄ – 8 ₃₅	125.35683	p-H ₂ O 4 ₀₄ – 3 ₁₃
126.71711	p-H ₂ O 3 ₃₁ – 3 ₂₂	130.32199	p-H ₂ O 7 ₅₃ – 8 ₂₆
137.68652	p-H ₂ O 7 ₃₅ – 8 ₀₈	138.53127	p-H ₂ O 3 ₁₃ – 2 ₀₂
138.64412	p-H ₂ O 8 ₄₄ – 7 ₅₃	144.52144	p-H ₂ O 4 ₁₃ – 3 ₂₂
146.92643	p-H ₂ O 4 ₃₁ – 4 ₂₂	148.71156	p-H ₂ O 8 ₃₅ – 8 ₂₆
148.79410	p-H ₂ O 5 ₄₂ – 6 ₁₅	156.19792	p-H ₂ O 3 ₂₂ – 3 ₁₃
158.31551	p-H ₂ O 3 ₃₁ – 4 ₀₄	159.48926	p-H ₂ O 8 ₂₆ – 9 ₁₉
167.03912	p-H ₂ O 6 ₂₄ – 6 ₁₅	169.74305	p-H ₂ O 7 ₃₅ – 6 ₄₂
170.14342	p-H ₂ O 6 ₃₃ – 6 ₂₄	174.61126	p-H ₂ O 5 ₃₃ – 6 ₀₆
187.11543	p-H ₂ O 4 ₁₃ – 4 ₀₄	208.08146	p-H ₂ O 7 ₂₆ – 6 ₃₃
208.91861	p-H ₂ O 9 ₄₆ – 10 ₁₉	222.95328	p-H ₂ O 7 ₄₄ – 8 ₁₇
243.98004	p-H ₂ O 2 ₂₀ – 2 ₁₁	248.25302	p-H ₂ O 4 ₂₂ – 4 ₁₃
251.75737	p-H ₂ O 8 ₅₃ – 7 ₆₂	255.68729	p-H ₂ O 7 ₄₄ – 6 ₅₁
269.27908	p-H ₂ O 1 ₁₁ – 0 ₀₀	303.46381	p-H ₂ O 2 ₀₂ – 1 ₁₁
308.97175	p-H ₂ O 5 ₂₄ – 4 ₃₁	327.23126	p-H ₂ O 4 ₂₂ – 3 ₃₁
330.82984	p-H ₂ O 9 ₂₈ – 8 ₃₅	398.65260	p-H ₂ O 2 ₁₁ – 2 ₀₂
613.72660	p-H ₂ O 6 ₂₄ – 7 ₁₇	631.57098	p-H ₂ O 5 ₃₃ – 4 ₄₀
636.66801	p-H ₂ O 6 ₄₂ – 5 ₅₁		

TABLE 6: Line list for single Gaussian fitting: ^{12}CO and ^{13}CO

^{12}CO		^{13}CO	
Wavelength (μm)	Line name	Wavelength (μm)	Line name
54.98622	$^{12}\text{CO J} = 48 - 47$	209.48144	$^{13}\text{CO J} = 13 - 12$
56.12190	$^{12}\text{CO J} = 47 - 46$	226.90368	$^{13}\text{CO J} = 12 - 11$
57.30773	$^{12}\text{CO J} = 46 - 45$	247.49662	$^{13}\text{CO J} = 11 - 10$
58.54705	$^{12}\text{CO J} = 45 - 44$	272.21148	$^{13}\text{CO J} = 10 - 9$
59.84349	$^{12}\text{CO J} = 44 - 43$	302.42221	$^{13}\text{CO J} = 9 - 8$
61.20106	$^{12}\text{CO J} = 43 - 42$	340.18978	$^{13}\text{CO J} = 8 - 7$
62.62410	$^{12}\text{CO J} = 42 - 41$	388.75282	$^{13}\text{CO J} = 7 - 6$
64.11741	$^{12}\text{CO J} = 41 - 40$	453.50906	$^{13}\text{CO J} = 6 - 5$
65.68791	$^{12}\text{CO J} = 40 - 39$	544.17444	$^{13}\text{CO J} = 5 - 4$
67.33814	$^{12}\text{CO J} = 39 - 38$		
69.07614	$^{12}\text{CO J} = 38 - 37$		
70.90902	$^{12}\text{CO J} = 37 - 36$		
72.84469	$^{12}\text{CO J} = 36 - 35$		
74.89194	$^{12}\text{CO J} = 35 - 34$		
77.06064	$^{12}\text{CO J} = 34 - 33$		
79.36181	$^{12}\text{CO J} = 33 - 32$		
81.80787	$^{12}\text{CO J} = 32 - 31$		
84.41284	$^{12}\text{CO J} = 31 - 30$		
87.19261	$^{12}\text{CO J} = 30 - 29$		
90.16527	$^{12}\text{CO J} = 29 - 28$	173.63580	$^{12}\text{CO J} = 15 - 14$
93.35147	$^{12}\text{CO J} = 28 - 27$	186.00397	$^{12}\text{CO J} = 14 - 13$
104.44758	$^{12}\text{CO J} = 25 - 24$	200.27751	$^{12}\text{CO J} = 13 - 12$
108.76555	$^{12}\text{CO J} = 24 - 23$	216.93275	$^{12}\text{CO J} = 12 - 11$
113.46045	$^{12}\text{CO J} = 23 - 22$	236.61924	$^{12}\text{CO J} = 11 - 10$
118.58370	$^{12}\text{CO J} = 22 - 21$	260.24634	$^{12}\text{CO J} = 10 - 9$
124.19648	$^{12}\text{CO J} = 21 - 20$	289.12761	$^{12}\text{CO J} = 9 - 8$
130.37221	$^{12}\text{CO J} = 20 - 19$	325.23335	$^{12}\text{CO J} = 8 - 7$
137.19978	$^{12}\text{CO J} = 19 - 18$	371.65974	$^{12}\text{CO J} = 7 - 6$
144.78783	$^{12}\text{CO J} = 18 - 17$	433.56713	$^{12}\text{CO J} = 6 - 5$
153.27056	$^{12}\text{CO J} = 17 - 16$	520.24412	$^{12}\text{CO J} = 5 - 4$
162.81572	$^{12}\text{CO J} = 16 - 15$	650.26787	$^{12}\text{CO J} = 4 - 3$

TABLE 7: Line list for single Gaussian fitting: OH, HCO⁺, and CH⁺

OH		HCO ⁺ & CH ⁺	
Wavelength (μm)	Line name	Wavelength (μm)	Line name
55.89231	OH ${}^2\Pi_{1/2, 9/2}^+ - {}^2\Pi_{1/2, 7/2}^-$	210.28817	HCO ⁺ J = 16 – 15
55.95141	OH ${}^2\Pi_{1/2, 9/2}^- - {}^2\Pi_{1/2, 7/2}^+$	224.28136	HCO ⁺ J = 15 – 14
65.13337	OH ${}^2\Pi_{3/2, 9/2}^- - {}^2\Pi_{3/2, 7/2}^+$	240.27541	HCO ⁺ J = 14 – 13
65.28048	OH ${}^2\Pi_{3/2, 9/2}^+ - {}^2\Pi_{3/2, 7/2}^-$	258.73207	HCO ⁺ J = 13 – 12
71.17262	OH ${}^2\Pi_{1/2, 7/2}^- - {}^2\Pi_{1/2, 5/2}^+$	280.26712	HCO ⁺ J = 12 – 11
71.21723	OH ${}^2\Pi_{1/2, 7/2}^+ - {}^2\Pi_{1/2, 5/2}^-$	305.71952	HCO ⁺ J = 11 – 10
79.11754	OH ${}^2\Pi_{1/2, 1/2}^- - {}^2\Pi_{3/2, 3/2}^+$	336.26531	HCO ⁺ J = 10 – 9
79.18106	OH ${}^2\Pi_{1/2, 1/2}^+ - {}^2\Pi_{3/2, 3/2}^-$	373.60195	HCO ⁺ J = 9 – 8
84.42237	OH ${}^2\Pi_{3/2, 7/2}^+ - {}^2\Pi_{3/2, 5/2}^-$	420.27521	HCO ⁺ J = 8 – 7
84.59877	OH ${}^2\Pi_{3/2, 7/2}^- - {}^2\Pi_{3/2, 5/2}^+$	480.28810	HCO ⁺ J = 7 – 6
115.15057	OH ${}^2\Pi_{1/2, 5/2}^+ - {}^2\Pi_{3/2, 7/2}^-$	560.30913	HCO ⁺ J = 6 – 5
115.38441	OH ${}^2\Pi_{1/2, 5/2}^- - {}^2\Pi_{3/2, 7/2}^+$	60.24659	CH ⁺ J = 6 – 5
119.23740	OH ${}^2\Pi_{3/2, 5/2}^- - {}^2\Pi_{3/2, 3/2}^+$	72.13950	CH ⁺ J = 5 – 4
119.44450	OH ${}^2\Pi_{3/2, 5/2}^+ - {}^2\Pi_{3/2, 3/2}^-$	119.85466	CH ⁺ J = 3 – 2
134.84152	OH ${}^2\Pi_{1/2, 7/2}^- - {}^2\Pi_{3/2, 9/2}^+$	358.99894	CH ⁺ J = 1 – 0
135.95981	OH ${}^2\Pi_{1/2, 7/2}^+ - {}^2\Pi_{3/2, 9/2}^-$		
154.78349	OH ${}^2\Pi_{1/2, 9/2}^+ - {}^2\Pi_{3/2, 11/2}^-$		
157.80984	OH ${}^2\Pi_{1/2, 9/2}^- - {}^2\Pi_{3/2, 11/2}^+$		
163.12467	OH ${}^2\Pi_{1/2, 3/2}^+ - {}^2\Pi_{1/2, 1/2}^-$		
163.40013	OH ${}^2\Pi_{1/2, 3/2}^- - {}^2\Pi_{1/2, 1/2}^+$		

Note—The notation of OH transition follows the form of ${}^2\Pi_{J_e, J_{\text{total}}}^{\text{parity}}$. J_e is the electron angular momentum quantum number, while J_{total} is the total angular momentum quantum number including electron and nuclear rotation. Please see more detail of the 163.12467 μm OH line in Section 5.1.

TABLE 8: Line list for single Gaussian fitting: atomic fine-structure lines

Wavelength (μm)	Line name	Wavelength (μm)	Line name
63.18367	[O I] ${}^3P_1 - {}^3P_2$	121.9	[N II] ${}^3P_2 - {}^3P_1$
145.48056	[O I] ${}^3P_2 - {}^3P_1$	157.69228	[C II] ${}^2P_{3/2} - {}^2P_{1/2}$
205.178	[N II] ${}^3P_1 - {}^3P_0$	230.34913	[C I] ${}^3P_2 - {}^3P_0$
370.42438	[C I] ${}^3P_2 - {}^3P_1$	609.15069	[C I] ${}^3P_1 - {}^3P_0$

TABLE 9: Blended lines fit with double Gaussian profile

Wavelength (μm)		Line name	
55.85970	55.89231	p-H ₂ O 6 ₅₁ – 7 ₂₆	OH ${}^2\Pi_{1/2, 9/2}^+ - {}^2\Pi_{1/2, 7/2}^-$
55.95141	55.98480	OH ${}^2\Pi_{1/2, 9/2}^- - {}^2\Pi_{1/2, 7/2}^+$	p-H ₂ O 7 ₇₁ – 7 ₆₂
56.77240	56.81777	p-H ₂ O 9 ₁₉ – 8 ₀₈	o-H ₂ O 9 ₀₉ – 8 ₁₈
65.13337	65.16779	OH ${}^2\Pi_{3/2, 9/2}^- - {}^2\Pi_{3/2, 7/2}^+$	o-H ₂ O 6 ₂₅ – 5 ₁₄
71.17262	71.21723	OH ${}^2\Pi_{1/2, 7/2}^- - {}^2\Pi_{1/2, 5/2}^+$	OH ${}^2\Pi_{1/2, 7/2}^+ - {}^2\Pi_{1/2, 5/2}^-$
75.81532	75.83188	p-H ₂ O 7 ₅₃ – 7 ₄₄	o-H ₂ O 6 ₅₂ – 6 ₄₃
79.11754	79.18106	OH ${}^2\Pi_{1/2, 1/2}^- - {}^2\Pi_{3/2, 3/2}^+$	OH ${}^2\Pi_{1/2, 1/2}^+ - {}^2\Pi_{3/2, 3/2}^-$
84.41284	84.42237	¹² CO J = 31 – 30	OH ${}^2\Pi_{3/2, 7/2}^+ - {}^2\Pi_{3/2, 5/2}^-$
113.46045	113.54021	¹² CO J = 23 – 22	o-H ₂ O 4 ₁₄ – 3 ₀₃
118.40826	118.58370	p-H ₂ O 9 ₃₇ – 8 ₄₄	¹² CO J = 22 – 21
130.32199	130.37221	¹² CO J = 20 – 19	p-H ₂ O 7 ₅₃ – 8 ₂₆
134.84152	134.93863	OH ${}^2\Pi_{1/2, 7/2}^- - {}^2\Pi_{3/2, 9/2}^+$	o-H ₂ O 5 ₁₄ – 5 ₀₅
156.19792	156.26908	p-H ₂ O 3 ₂₂ – 3 ₁₃	o-H ₂ O 5 ₂₃ – 4 ₃₂
144.52144	144.78783	p-H ₂ O 4 ₁₃ – 3 ₂₂	¹² CO J = 18 – 17
166.81885	167.03912	o-H ₂ O 7 ₃₄ – 7 ₂₅	p-H ₂ O 6 ₂₄ – 6 ₁₅
174.61126	174.63028	p-H ₂ O 5 ₃₃ – 6 ₀₆	o-H ₂ O 3 ₀₃ – 2 ₁₂
259.98875	260.24634	o-H ₂ O 3 ₁₂ – 2 ₂₁	¹² CO J = 10 – 9
272.21148	273.19988	¹³ CO J = 10 – 9	o-H ₂ O 3 ₁₂ – 3 ₀₃
302.42221	303.46381	¹³ CO J = 9 – 8	p-H ₂ O 2 ₀₂ – 1 ₁₁
370.42438	371.65974	[C I] ³ P ₂ – ³ P ₁	¹² CO J = 7 – 6
609.15069	613.72660	[C I] ³ P ₁ – ³ P ₀	p-H ₂ O 6 ₂₄ – 7 ₁₇

TABLE 10: Archive Sources

Source	Other Name	PACS OBSIDs	SPiRE OBSID	RA	Dec	Prog.	Jitter Corr.	SPiRE 1-D
AB Aur		1342217842, 1342217843		04h55m45.8s	+30d33m04.3s	D	x	
AS 205		1342215737, 1342215738		16h11m31.4s	-18d38m26s	D	x	
B1-a		1342216182, 1342216183	1342249475	03h33m16.7s	+31d07m55.2s	D,C	x	x
B1-c		1342216213, 1342216214	1342249476	03h33m17.9s	+31d09m31.9s	D,C	x	x
B335		1342208889, 1342208888	1342253652	19h37m00.9s	+07d34m09.7s	D,C	x	x
BHR 71		1342212230, 1342212231	1342248249	12h01m36.3s	-65d08m53.0s	D,C	x	x
Ced110-IRS4		1342225730, 1342225731	1342248246	11h06m47.0s	-77d22m32.4s	C		x
DG Tau				04h27m04.7s	+26d06m16s	D	x	
DK Cha	IRAS 12496-7650	1342188039, 1342188040	1342254037	12h53m17.2s	-77d07m10.7s	D,C	x	x
EC 82	[EC92] 82	1342192975, 1342219435		18h29m56.9s	+01d14m47s	D		
Elias 29		1342228519, 1342228520		16h27m09.4s	-24d37m18.6s	D	x	x
FU Ori		1342250907, 1342250908	1342230412	05h45m22.4s	+09d04m12s	F	x	x
GSS30-IRS1		1342215678, 1342215679	1342251286	16h26m21.4s	-24d23m04.3s	D,C	x	x
HD 100453		1342211695, 1342211696		11h33m05.6s	-54d19m29s	D	x	

Source	Other Name	PACS OBSIDs	SPIRE OBSID	RA	Dec	Prog.	Jitter Corr.	SPIRE 1-D
HD 100546		1342188037, 1342188038		11h33m25.4s	-70d11m41s	D	x	
HD 104237		1342207819, 1342207820		12h00m05.1s	-78d11m35s	D	x	
HD 135344		1342213921, 1342213922		15h15m49.0s	-37d08m56s	D	x	
HD 139614		1342215683, 1342215684		15h40m46.4s	-42d29m54s	D	x	
HD 141569		1342213913		15h49m57.8s	-03d55m16s	D	x	
HD 142527		1342216174, 1342216175		15h56m41.9s	-42d19m23s	D	x	
HD 142666		1342213916		15h56m40.0s	-22d01m40s	D		
HD 144432		1342213919		16h06m58.0s	-27d43m10s	D	x	
HD 144668		1342215641, 1342215642		16h08m34.3s	-39h06m18s	D	x	
HD 150193		1342227068		16h40m17.9s	-23d53m45s	D	x	
HD 163296		1342217819, 1342217820		17h56m21.3s	-21d57m22s	D	x	
HD 169142		1342206987, 1342206988		18h24m29.8s	-29d46m49s	D	x	
HD 179218		1342208884, 1342208885		19h11m11.3s	+15d47m16s	D	x	
HD 203024		1342206975		21h16m03.0s	+68d54m52s	D		
HD 245906		1342228528		05h39m30.5s	+26d19m55s	D		
HD 35187		1342217846		05h24m01.2s	+24d57m38s	D	x	
HD 36112		1342228247, 1342228248		05h30m27.5s	+25d19m57s	D	x	
HD 38120		1342226212, 1342226213		05h43m11.9s	-04d59m50s	D	x	

Source	Other Name	PACS OBSIDs	SPiRE OBSID	RA	Dec	Prog.	Jitter Corr.	SPiRE 1-D
HD 50138		1342206991, 1342206992		06h51m33.4s	-06d57m59s	D	x	
HD 97048		1342199412, 1342199413		11h08m03.3s	-77d39m18s	D	x	
HD 98922		1342210385		11h22m31.7s	-53d22m12s	D		
HH 100			1342252897	19h01m49.1s	-36d58m16.0s	C		
HH 46			1342245084	08h25m43.9s	-51d00m36.0s	C		x
HT Lup		1342213920		15h45m12.9s	-34d17m31s	D		
IRAM 04191+1522		1342216654, 1342216655		04h21m56.9s	+15d29m45.9s	D		
IRAS 03245+3002	L1455-IRS1	1342214677, 1342214676	1342249053	03h27m39.1s	+30d13m03.1s	D,C	x	x
IRAS 03301+3111	Perseus Bolo76	1342215668, 1342216181	1342249477	03h33m12.8s	+31d21m24.2s	D,C	x	x
IRAS 15398-3359	B228	1342228474, 1342228475	1342250515	15h43m01.3s	-34d09m15.0s	C		x
IRS 46 / IRS44	Oph-IRS44/46		1342251289	16h27m29.4s	-24d39m16.1s	D,C		
IRS 48	Oph-IRS48	1342227069, 1342227070		16h27m37.2s	-24d30m35s	D		x
IRS 63	Oph-IRS63	1342228473, 1342228472		16h31m35.6s	-24d01m29.3s	D		x
L1014		1342208911, 1342208912	1342245857	21h24m07.5s	+49d59m09.0s	D,C		x
L1157		1342208909, 1342208908	1342247625	20h39m06.3s	+68d02m16.0s	D,C	x	x
L1448-MM		1342213683, 1342214675		03h25m38.9s	+30d44m05.4s	D		x
L1455-IRS3	IRAS 03249+2957	1342204122, 1342204123	1342249474	03h28m00.4s	+30d08m01.3s	D,C		x

Source	Other Name	PACS OBSIDs	SPiRE OBSID	RA	Dec	Prog.	Jitter Corr.	SPiRE 1-D
L1489	IRAS 04016+2610	1342216216, 1342216215		04h04m42.9s	+26d18m56.3s	D	x	
L1527	IRAS 04368+2557	1342192981, 1342192982		04h39m53.9s	+26d03m09.8s	D	x	
L1551-IRS5		1342192805, 1342229711	1342249470	04h31m34.1s	+18d08m04.9s	D,C	x	x
L483	IRAS 18140-0440		1342253649	18h17m29.9s	-04d39m39.5s	C		x
L723-MM			1342245094	19h17m53.7s	+19d12m20.0s	C		x
RCrA-IRS5A		1342207806, 1342207805	1342253646	19h01m48.1s	-36d57m22.7s	D,C		x
RCrA-IRS7B		1342207807, 1342207808	1342242620	19h01m56.4s	-36d57m28.3s	D,C	x	x
RCrA-IRS7C		1342206990, 1342206989	1342242621	19h01m55.3s	-36d57m17.0s	D,C		x
RNO 90		1342228206		16h34m09.2s	-15d48m17s	D	x	
RNO 91			1342251285	16h34m29.3s	-15d47m01.4s	C		x
RU Lup		1342215682		15h56m42.3s	-37d49m16s	D	x	
RY Lup		1342216171		15h59m28.4s	-40d21m51s	D	x	
S Cra		1342207809, 1342207810		19h01m08.6s	-36d57m20s	D	x	
Serpens-SMM3		1342193216, 1342193214		18h29m59.3s	+01d14m01.7s	D	x	
Serpens-SMM4		1342193217, 1342193215		18h29m56.7s	+01d13m17.2s	D		
SR 21		1342227209, 1342227210		16h27m10.3s	-24d19m13s	D	x	
TMC 1A	IRAS 04362+2535	1342192987, 1342192988	1342250510	04h39m35.0s	+25d41m45.5s	D,C	x	x
TMC 1	IRAS 04381+2540	1342225803, 1342225804	1342250512	04h41m12.7s	+25d46m35.9s	D,C	x	x

Source	Other Name	PACS OBSIDs	SPIRE OBSID	RA	Dec	Prog.	Jitter Corr.	SPIRE 1-D
TMR 1	IRAS 04361+2547	1342192985, 1342192986	1342250509	04h39m13.9s	+25d53m20.6s	D,C	x	x
V1057 Cyg		1342235853, 1342235852	1342221695	20h58m53.7s	+44d15m29s	F	x	x
V1331 Cyg		1342233446, 1342233445	1342221694	21h01m09.2s	+50d21m45s	F	x	x
V1515 Cyg		1342235691, 1342235690	1342221685	20h23m48.0s	+42d12m26s	F	x	x
V1735 Cyg	Elias 1-12	1342235849, 1342235848	1342219560	21h47m20.7s	+47d32m04s	F	x	
VLA1623-243		1342213918, 1342213917	1342251287	16h26m26.4s	-24d24m30.0s	D,C	x	x
WL 12		1342228187, 1342228188	1342251290	16h26m44.2s	-24d34m48.4s	D,C	x	x

TABLE 10: Contents of the archive organized by source. The ‘Prog.’ column refers to the first program in which the source was observed, where D = DIGIT, F = FOOSH, and C = COPS. The ‘Jitter Corr.’ column indicates the accessibility of the jitter corrected data. Sources with an ‘x’ in this column have and fitted with jitter-corrected products. The ‘SPIRE 1-D’ column indicates the accessibility of SPIRE extended calibrated 1-D spectra.

8 References

- Authier, N., Bagland, N., & Lefloch, A. 1993, *Journal of Molecular Spectroscopy*, 160, 590
- Cieza, L. A., Olofsson, J., Harvey, P. M., et al. 2013, *Astrophysical Journal*, 762, 100
- Goorvitch, D. 1994, *Astrophysical Journal Supplement Series*, 95, 535
- Green, J. D., Evans, II, N. J., Kóspál, Á., et al. 2013a, *Astrophysical Journal*, 772, 117
- Green, J. D., Evans, II, N. J., Jørgensen, J. K., et al. 2013b, *Astrophysical Journal*, 770, 123
- Griffin, M. J., Abergel, A., Abreu, A., et al. 2010, *Astronomy & Astrophysics*, 518, L3+
- Je, H., Lee, J.-E., Lee, S., Green, J. D., & Evans, II, N. J. 2015, ArXiv e-prints, arXiv:1501.05048
- Karska, A., Herczeg, G. J., van Dishoeck, E. F., et al. 2013, *Astronomy & Astrophysics*, 552, A141
- Kristensen, L. E., van Dishoeck, E. F., Bergin, E. A., et al. 2012, *Astronomy & Astrophysics*, 542, A8
- Lahuis, F., Kessler-Silacci, J. E., Knez, C., et al. 2006, *c2d Spectroscopy Explanatory Supplement*. (Pasadena, CA: Spitzer Science Center)
- Lee, J., Lee, J.-E., Lee, S., et al. 2013, *Astrophysical Journal Supplement Series*, 209, 4
- Markwardt, C. B. 2009, in *Astronomical Society of the Pacific Conference Series*, Vol. 411, *Astronomical Data Analysis Software and Systems XVIII*, ed. D. A. Bohlender, D. Durand, & P. Dowler, 251
- Müller, H., Schlöder, F., Stutzki, J., & Winnewisser, G. 2005, *Journal of Molecular Structure*, 742, 215
- Nisini, B., Benedettini, M., Codella, C., et al. 2010, *Astronomy & Astrophysics*, 518, L120
- Palla, F., & Stahler, S. W. 1993, *Astrophysical Journal*, 418, 414
- Poglitsch, A., Waelkens, C., Geis, N., et al. 2010, *Astronomy & Astrophysics*, 518, L2
- Schöier, F. L., van der Tak, F. F. S., van Dishoeck, E. F., & Black, J. H. 2005, *Astronomy & Astrophysics*, 432, 369
- van Dishoeck, E. F., Kristensen, L. E., Benz, A. O., et al. 2011, *PASP*, 123, 138
- Wampfler, S. F., Bruderer, S., Karska, A., et al. 2013, *Astronomy & Astrophysics*, 552, A56
- Ward-Thompson, D., André, P., Crutcher, R., et al. 2007, *Protostars and Planets V*, 33